VICON: Vision In-Context Operator Networks for Multi-Physics Fluid Dynamics Prediction

Anonymous Author(s)
Affiliation
Address
email

Abstract

In-Context Operator Networks (ICONs) have demonstrated the ability to learn operators across diverse partial differential equations using few-shot, in-context learning. However, existing ICONs process each spatial point as an individual token, severely limiting computational efficiency when handling dense data in higher spatial dimensions. We propose *Vision In-Context Operator Networks* (VICON), which integrates vision transformer architectures to efficiently process 2D data through patch-wise operations while preserving ICON's adaptability to multiphysics systems and varying timesteps. Evaluated across three fluid dynamics benchmarks, VICON significantly outperforms state-of-the-art baselines: DPOT and MPP, reducing the averaged last-step rollout error by 37.9% compared to DPOT and 44.7% compared to MPP, while requiring only 72.5% and 34.8% of their respective inference times. VICON naturally supports flexible rollout strategies with varying timestep strides, enabling immediate deployment in *imperfect measurement systems* where sampling frequencies may differ or frames might be dropped—common challenges in real-world settings—without requiring retraining or interpolation. In these realistic scenarios, VICON exhibits remarkable robustness, experiencing only 24.41% relative performance degradation compared to 71.37%-74.49% degradation in baseline methods, demonstrating its versatility for depolying in realistic applications.

1 Introduction

Machine learning has emerged as a powerful tool for solving Partial Differential Equations (PDEs). Traditional approaches primarily operate on discrete representations, with Convolutional Neural Networks (CNNs) excelling at processing regular grids [1], Graph Neural Networks (GNNs) handling unstructured meshes [2, 3, 4], and transformers capturing dependencies between sampling points within the same domains [5, 6, 7]. However, these discrete approaches face a fundamental limitation: they lack PDE context information (such as governing parameters) and consequently cannot generalize to new parameters or PDEs beyond their training set.

This limitation led to the development of "operator learning," where neural networks learn mappings from input functions to output functions, such as from initial/boundary conditions to PDE solutions. This capability was first demonstrated using shallow neural networks [8, 9], followed by specialized architectures including the widely-adopted Deep Operator Network (DeepONet) [10], Fourier Neural Operator (FNO) [11, 12], and recent transformer-based operator learners [13, 14, 15]. While these methods excel at learning individual parametric PDEs, they cannot generalize across different PDE types, necessitating costly retraining for new equations or even different time step sizes.

Inspired by the success of large language models in multi-domain generation, researchers have explored "Multi-Physics PDE models" to address this single-operator limitation. Common approaches

Submitted to 39th Conference on Neural Information Processing Systems (NeurIPS 2025). Do not distribute.

employ pre-training and fine-tuning strategies [16, 17, 18], though these require substantial additional data (typically hundreds of frames) and fine-tuning before deployment. This requirement severely limits their practical applications in scenarios like online control and data assimilation, where rapid adaptation with limited data sampling is essential.

To eliminate the need for additional data collection and fine-tuning, several works have attempted to achieve few-shot or zero-shot generalization across multi-physics systems by incorporating explicit PDE information. For example, the PROSE approach [19, 20, 21, 22] processes the symbolic form of governing equations using an additional transformer branch. Similarly, PDEformer [23] converts PDEs into directed graphs as input for graph transformers, while others embed symbol-tokens directly into the model [24]. Despite these advances, such methods require explicit knowledge of the underlying PDEs, which is often unavailable when deploying models in new environments.

To further lower barriers for applying multi-physics models in real-world applications, the In-Context Operator Network (ICON) [25] offers a fundamentally different approach: ICON implicitly encodes system dynamics through a few input-output function pairs, then extracts dynamics from these pairs in an in-context fashion. This approach enables few-shot generalization without retraining or explicit PDE knowledge, while the minimal required input-output pairs can be readily collected during deployment. A single ICON model has demonstrated success in handling both forward and inverse problems across various ODEs, PDEs, and mean field control scenarios.

However, ICON's computational efficiency becomes a critical bottleneck when handling dense data in higher dimensions. Specifically, ICON treats each sampled spatial point as an individual token, leading to quadratic computational complexity with respect to the number of points. This makes it computationally prohibitive for practical 2D and 3D applications—to date, only one instance of a 2D case using sparse data points has been demonstrated [25].

To address this limitation, we propose *Vision In-Context Operator Networks* (VICON), which leverage vision transformers to process 2D functions using an efficient patch-wise approach. Going beyond classic vision transformers that typically process patches from a single image, VICON extends the architecture to handle sequences of input-output function pairs, enabling "next function prediction" capabilities while preserving the benefits of in-context operator learning.

Our contributions include:

- Development of VICON, a vision transformer-based in-context operator network for two-dimensional time-dependent PDEs that maintains the flexibility of in-context operator learning while efficiently handling dense data in higher dimensions.
- Comprehensive evaluation across diverse fluid dynamics systems comprising 879K frames with varying timestep sizes, demonstrating substantial improvements over state-of-the-art models MPP [26] and DPOT [27] in both accuracy and efficiency. Our approach reduces the averaged last-step rollout error by 37.9% compared to DPOT and 44.7% compared to MPP, while requiring only 72.5% and 34.8% of their respective inference times.
- Enhanced flexibility supporting varying timestep strides and non-sequential measurements, offering substantial robustness in realistic scenarios with imperfect data collection, e.g. with missing frames. Under these scenarios, VICON exhibits only 24.41% relative performance degradation versus 71.37%-74.49% degradation in baseline methods.

2 Related Works

Operator Learning. Operator learning [8, 9, 11, 10] addresses the challenge of approximating operators $G : U \to V$, where U and V are function spaces representing physical systems and differential equations, e.g., G maps initial/boundary conditions or system parameters to corresponding solutions. Among the various operator learning approaches, DeepONets [10, 28] employ branch and trunk networks to independently process inputs and query points, while FNOs [11] leverage fast Fourier transforms to efficiently compute kernel integrations for PDE solutions in regular domains. These methods have been extended to incorporate equation information [29, 30], multiscale features [31, 32, 33], adaptation to heterogeneous and irregular meshes [34, 35, 36, 37].

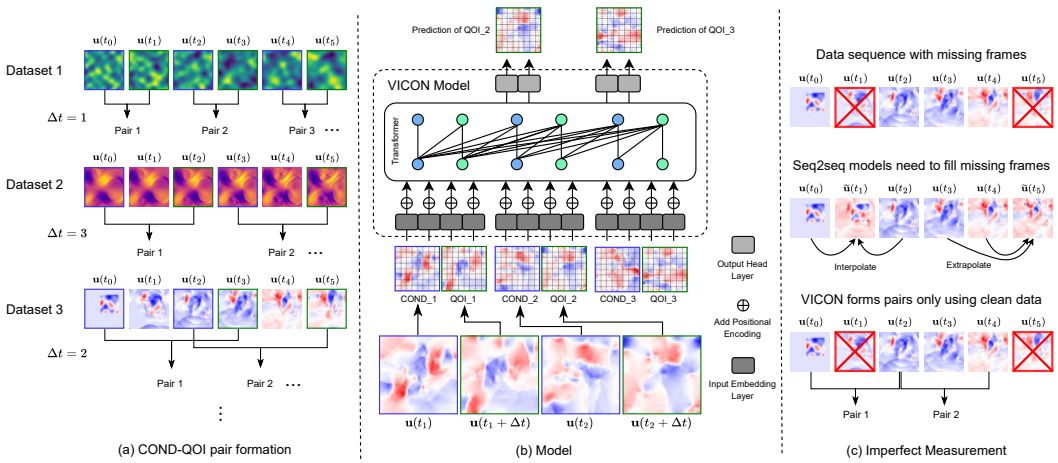

Figure 1: **VICON model overview.** (a) The formation process for conditions (COND) and quantities of interest (QOI) pairs. Δt is randomly sampled during training. (b) Model illustration. The inputs to the model are pairs of COND and QOI, which are patchified and flattened before feeding into the transformer layers. The outputs, which represent different patches in the output frame, are transformed back to obtain the final predictions. (c) With imperfect temporal measurements, VICON forms pairs using only clean data, and does not need to fill missing frames.

However, these approaches typically learn a single operator, requiring retraining when encountering different PDE types or time-step sizes. Our work aims to develop a unified model for multiple PDEs with few-shot generalization capabilities based on limited observation frames.

Multi-Physics PDE Models. Foundation models in natural language processing [38, 39] and computer vision [40] have demonstrated remarkable versatility across diverse tasks. Drawing inspiration from this paradigm, recent research has explored developing unified models for multiple PDEs in domains such as PDE discovery [41] and computational fluid dynamics [42]. Several approaches follow pre-training and fine-tuning strategies [16, 17], though these require additional resources for data acquisition and fine-tuning before deployment. In parallel, researchers have developed zero- or few-shot multi-physics models by incorporating additional information; for instance, the PROSE approach [19, 20, 21, 22, 43] directly encodes symbolic information of PDEs into the model. Other methods achieving zero- or few-shot generalization include using physics-informed tokens [24], representing PDE structures as graphs [23], or conditioning transformers on PDE descriptions [44]; however, all these techniques require prior knowledge of the PDEs as additional inputs. We select two state-of-the-art models, MPP [26] and DPOT [27], as our baselines.

In-Context Operator Networks. ICONs [25, 45, 46] learn operators by observing input-output function pairs, enabling few-shot generalization across various PDEs without requiring explicit PDE representations or fine-tuning. These networks have demonstrated success in handling forward and inverse problems for ODEs, PDEs, and mean-field control scenarios. However, ICONs face significant computational challenges when processing dense data, as they represent functions through scattered point tokens, resulting in quadratic computational complexity with respect to the number of sample points. This limitation has largely restricted their application to 1D problems, with only sparse sampling feasible in 2D cases [25]. Our work addresses these limitations by introducing a vision transformer architecture that efficiently handles dense 2D data while preserving the benefits of in-context operator learning.

3 Preliminaries

ICONs were introduced and developed in [25, 45, 46]. They adapt the in-context learning framework from large language models, aiming to train a model that can learn operators from prompted function examples.

Denote an ICON model as $\mathcal{T}_\theta$, where $\mathcal{T}$ is a transformer with trainable parameters θ. The model takes input as a sequence comprising I pairs of conditions ($\boldsymbol{c}$) and quantities of interest ($\boldsymbol{q}$) as $\{\langle \boldsymbol{c}_i, \boldsymbol{q}_i \rangle\}_{i=1}^I$, where each $\boldsymbol{c}, \boldsymbol{q}$ contains multiple tokens representing a single function. The model outputs tokens representing future functions at the positions of $\boldsymbol{c}$, i.e. "next function prediction" similar to "next token predictions" in LLM. More precisely, for $J \in \{1, \ldots, I-1\}$, the model predicts $\tilde{\boldsymbol{q}}_{J+1}$ given the leading J pairs and the condition $\boldsymbol{c}_{J+1}$:

$$\tilde{\boldsymbol{q}}_{J+1} = \mathcal{T}_\theta[\boldsymbol{c}_{J+1}; \{\langle \boldsymbol{c}_i, \boldsymbol{q}_i \rangle\}_{i=1}^J]. \tag{1}$$

For training parallelization, ICON uses a special causal attention mask to perform autoregressive learning (i.e., the model only sees the leading J pairs and $\boldsymbol{c}_{J+1}$ when predicting $\tilde{\boldsymbol{q}}_{J+1}$) and enables output of all predictions within a single forward pass [45]:

$$\{\tilde{\boldsymbol{q}}_i\}_{i=1}^I = \mathcal{T}_\theta[\{\langle \boldsymbol{c}_i, \boldsymbol{q}_i \rangle\}_{i=1}^I]. \tag{2}$$

Training loss is computed as the mean squared error (MSE) between the predicted states $\tilde{\boldsymbol{q}}_i$ and the ground truth states $\boldsymbol{q}_i$. To ensure that the model receives sufficient contextual information about the underlying dynamics, we only compute errors for the indices $i > I_{\text{min}}$, effectively requiring at least I_{min} examples in context. This approach has shown empirical improvements in model performance.

After training, ICON can process a new set of $\langle \boldsymbol{c}, \boldsymbol{q} \rangle$ pairs in the forward pass to in-contextually learn operators and employ them to predict future functions using new conditions:

$$\tilde{\boldsymbol{q}}_k = \mathcal{T}_\theta[\boldsymbol{c}_k; \{\langle \boldsymbol{c}_i, \boldsymbol{q}_i \rangle\}_{i=1}^J], \tag{3}$$

where $J \in \{I_{\text{min}}, \ldots, I-1\}$ is the number of in-context examples, I_{min} is the number of context exempted from loss calculation, and $k > I$ is the index of the condition for future prediction.

Importantly, all pairs in the same sequence must be formed with the same operator mapping (i.e., the same PDE and consistent timestep size), while operators can vary across different sequences.

4 Methodology

4.1 Problem Setup

We consider the forward problem for multiple time-dependent PDEs that are *temporally homogeneous Markovian*, defined on domain $\Omega \subseteq \mathbb{R}^2$ with solutions represented by $\mathbf{u}(\boldsymbol{x}, t) : \Omega \times [0, T] \to \mathbb{R}^c$, where c is the number of channels. Given the initial I_0 frames, $\{\mathbf{u}_i = \mathbf{u}(\cdot, t_i) \mid i = 1, \ldots, I_0\}$, the task is to predict future solutions.

Each solution frame is discretized as a three-dimensional tensor $\mathbf{u}_t = \mathbf{u}(\cdot, t) \in \mathbb{R}^{N_x \times N_y \times c}$, where N_x and N_y are the spatial grid sizes. Due to the homogeneous Markovian property, given the initial data $\{\mathbf{u}_t \mid t \geq 0\}$ from some PDE indexed by i_p, for a fixed Δt, there exists an operator $\mathcal{L} = \mathcal{L}_{\Delta t}^{(i_p)}$ that maps frame $\mathbf{u}_t$ to frame $\mathbf{u}_{t+\Delta t}$ for any $t \geq 0$. Our goal is to train a model that learns these operators $\mathcal{L}_{\Delta t}^{(i_p)}$ from the sequence of function pairs generated from the initial frames. Notably, even within the same dataset and fixed Δt, different trajectories can exhibit different dynamics (e.g., due to different Reynolds numbers Re). These variations are implicitly captured by the function pairs in our framework.

4.2 Vision In-Context Operator Networks

The original ICONs represent functions as scattered sample data points, where each data point is projected as a single token. For higher spatial dimensions, this approach necessitates an excessively large number of sample points and extremely long sequences in the transformer. Due to the inherent quadratic complexity of the transformer, this approach becomes computationally infeasible for high-dimensional problems.

Inspired by the Vision Transformer (ViT) [47], we address these limitations by dividing the physical fields into patches, where each patch is flattened and projected as a token. This approach, which we call Vision In-Context Operator Networks (VICON), has its forward process illustrated in Figure 1(b) and detailed in the following.

First, the input $\boldsymbol{u}_t$ and output $\boldsymbol{u}_{t+\Delta t}$ functions are divided into patches $\{\boldsymbol{C}^k \in \mathbb{R}^{R_x \times R_y \times c}\}_{k=1}^{N_c}$ and $\{\boldsymbol{Q}^l \in \mathbb{R}^{R_x \times R_y \times c}\}_{l=1}^{N_q}$, where R_x, R_y are the resolution dimensions of the patch and N_c and N_q are the number of patches for the input and output functions, respectively. While N_q can differ from N_c (for instance, when input functions require additional boundary padding, resulting in $N_c > N_q$), we maintain $N_c = N_q$ throughout our experiments. For notational clarity, we add the subscript $i \in \{1, \ldots, I\}$ to denote the pair index, where $\boldsymbol{C}_i^k$ represents the k-th patch of the input function and $\boldsymbol{Q}_i^l$ represents the l-th patch of the output function in the i-th pair. These patches are then projected into a unified d-dimensional latent embedding space using a shared learnable linear function $f_\phi : R_x \times R_y \times c \to \mathbb{R}^d$:

$$\hat{\boldsymbol{c}}_i^k = f_\phi(\boldsymbol{C}_i^k), \quad \hat{\boldsymbol{q}}_i^l = f_\phi(\boldsymbol{Q}_i^l), \tag{4}$$

where $k = 1, \ldots, N_c$ and $l = 1, \ldots, N_q$ are the index of patches.

We inject two types of learnable positional encoding before feeding the embeddings into the transformer: (1) patch positional encodings to indicate relative patch positions inside the whole domain, denoted as $\mathbf{E}_p \in \mathbb{R}^{N_p \times d}$, where $N_p = \max\{N_c, N_q\}$; (2) function positional encodings to indicate whether a patch belongs to a input function (using $\mathbf{E}_c \in \mathbb{R}^{I \times d}$) or output function (using $\mathbf{E}_q \in \mathbb{R}^{I \times d}$), as well as their indices in the sequence:

$$\boldsymbol{c}_i^k = \hat{\boldsymbol{c}}_i^k + \mathbf{E}_p(k) + \mathbf{E}_c(i), \quad \boldsymbol{q}_i^l = \hat{\boldsymbol{q}}_i^l + \mathbf{E}_p(l) + \mathbf{E}_q(i). \tag{5}$$

The embeddings $\boldsymbol{c}_i^k$ and $\boldsymbol{q}_i^l$ are then concatenated to form the input sequence for the transformer:

$$\mathbf{c}_1^1 \ldots \mathbf{c}_1^{N_c}, \mathbf{q}_1^1 \ldots \mathbf{q}_1^{N_q}, \ldots, \mathbf{c}_I^1 \ldots \mathbf{c}_I^{N_c}, \mathbf{q}_I^1 \ldots \mathbf{q}_I^{N_q}.$$

To support autoregressive prediction similar to Equation (2), VICON employs an alternating-sized (in the case where $N_c \neq N_q$) block causal attention mask, as opposed to the conventional triangular causal attention mask as in mainstream generative large language models [38] and large vision models [48]. The mask is defined as follows:

$$\mathbf{M} = \begin{bmatrix} \mathbf{1}_{N_c,N_c} & \mathbf{0} & \cdots & \mathbf{0} & \mathbf{0} \\ \mathbf{1}_{N_q,N_c} & \mathbf{1}_{N_q,N_q} & \cdots & \mathbf{0} & \mathbf{0} \\ \vdots & \vdots & \ddots & \vdots & \vdots \\ \mathbf{1}_{N_c,N_c} & \mathbf{1}_{N_c,N_q} & \cdots & \mathbf{1}_{N_c,N_c} & \mathbf{0} \\ \mathbf{1}_{N_q,N_c} & \mathbf{1}_{N_q,N_q} & \cdots & \mathbf{1}_{N_q,N_c} & \mathbf{1}_{N_q,N_q} \end{bmatrix} \tag{6}$$

where $\mathbf{1}_{m \times n}$ denotes an all-ones matrix of dimension $m \times n$, and $\mathbf{0}$ represents a zero matrix of the corresponding dimensions.

After obtaining the output tokens from Equation (2), we extract the tokens corresponding to the input patch indices $\mathbf{c}_i^1, \ldots, \mathbf{c}_i^{N_c}$ and denote them as $\tilde{\boldsymbol{q}}_i^1, \ldots, \tilde{\boldsymbol{q}}_i^{N_c}$. These tokens are then projected back to the original physical space using a shared learnable linear function $g_\psi : \mathbb{R}^d \to \mathbb{R}^{R_x \times R_y \times c}$:

$$\tilde{\boldsymbol{Q}}_i^l = g_\psi(\tilde{\boldsymbol{q}}_i^l), \tag{7}$$

which predicts $\boldsymbol{Q}_i^l$.

4.3 Prompt Normalization

To address the varying scales across different channels and prompts (i.e. sequences of pairs $\{\langle \boldsymbol{c}_i, \boldsymbol{q}_i \rangle\}_{i=1}^I$), we normalize the data before feeding them into the model. A crucial requirement is to consistently normalize functions within the same sequence, to ensure that the same operator is learned. Denoting the normalization operators for $\boldsymbol{c}$ and $\boldsymbol{q}$ as $\mathcal{N}_c$ and $\mathcal{N}_q$ respectively, and the operator in the original space as $\mathcal{L}$, the operator in the normalized space $\mathcal{L}'$ follows:

$$\mathcal{L}'(\mathcal{N}_c(\mathbf{u})) = \mathcal{N}_q(\mathcal{L}(\mathbf{u})). \tag{8}$$

In this work, we simply set $\mathcal{N}_c = \mathcal{N}_q$, mainly because our maximum timestep stride $s_{\text{max}} = 5$ is relatively small (i.e., the scale distribution does not change dramatically). Specifically, we computed the channel-wise mean μ and standard deviation σ of $\{\boldsymbol{c}_i\}_{i=1}^I$ in each prompt, then used these values to normalize $\{\langle \boldsymbol{c}_i, \boldsymbol{q}_i \rangle\}_{i=1}^I$ in that prompt. To avoid division by zero, we set a minimum threshold of 10^{-4} for the standard deviation.

4.4 Datasets and Data Augmentation

We evaluate on three fluid dynamics datasets representing different physical regimes: 1) PDEArena-Incomp [1] (incompressible Navier-Stokes equations), containing 2,496/608/608 trajectories (train/valid/test) with 56 timesteps each; 2) PDEBench-Comp-HighVis [49] (compressible Navier-Stokes with high viscosity), containing 40,000 trajectories of 21 timesteps each; and 3) PDEBench-Comp-LowVis [49] (compressible Navier-Stokes with numerically zero viscosity), containing 4,000 trajectories of 21 timesteps each. For PDEBench-Comp-HighVis and PDEBench-Comp-LowVis, we randomly split trajectories in 80%/10%/10% proportions for training/validation/testing, respectively.

The temporally homogeneous Markovian property (Section 4.1) enables natural data augmentation for training and flexible rollout strategy for inference (Section 4.5): by striding with larger timesteps to reduce the number of autoregressive steps in long-term prediction tasks: $\Delta t = s\Delta\tau_{i_p} \mid s = 1, 2, \ldots, s_{\text{max}}$, where τ_{i_p} is the timestep size for recording in trajectory i_p. During training, for each trajectory in the training set, we first sample a stride size $s \sim \mathcal{U}\{1, \ldots, s_{\text{max}}\}$, then form $\langle \mathbf{u}_t, \mathbf{u}_{t+s\Delta\tau} \rangle$ pairs for the corresponding operator. We illustrate this augmentation process in Figure 1(a), where different strides are randomly sampled during dataloading.

Additional dataset details appear in Appendix A.

4.5 Inference with Flexible Strategies

As mentioned in Section 4.4, VICON can make predictions with varying timestep strides. Given I_0 initial frames $\{\mathbf{u}_i\}_{i=1}^{I_0}$, we can form in-context example pairs $\{\langle \mathbf{u}_i, \mathbf{u}_{i+s} \rangle\}_{i=1}^{I_0-s}$. For $j \geq 1$, we set the question condition ($\boldsymbol{c}_k$ in Equation (3)) as $\boldsymbol{u}_j$ to predict $\boldsymbol{u}_{j+s}$, enabling s-step prediction.

For long-term rollout, we employ VICON in an autoregressive fashion. The ability to predict with different timestep strides enables various rollout strategies. We explore two natural approaches: single-step rollout and flexible-step rollout, where the latter advances in larger strides to reduce the number of rollout steps.

For single-step rollout, we simply follow the autoregressive procedure with $s = 1$. Flexible-step rollout involves a more sophisticated approach: given a maximum prediction stride s_{max}, we first make sequential predictions with a gradually growing $s = 1$ to s_{max} using $\mathbf{u}_{I_0}$ as the question condition, obtaining $\{\mathbf{u}_{I_0+s}\}_{s=1}^{s_{\text{max}}}$. Using each frame in this sequence as a question condition, we then make consistent s_{max}-step predictions while preserving all intermediate frames. This flexible-step strategy follows the approach in [46].

This strategy is also applicable to the imperfect measuring cases where partial input frames are missing, eg, due to sensor device error. In this case, we can still form pairs from the remaining frames, with minor adjustment to the strategy generation algorithms, as shown in Figure 1(c).

More details (including algorithms and examples) on rollout strategies are provided in Appendix C.1 (for perfect measurements) and in Appendix C.2 (for imperfect measurements).

4.6 Evaluation Metric

We evaluate the rollout accuracy of VICON using two different strategies described in Section 4.5. The evaluation uses relative and absolute L^2 errors between the predicted and ground truth frames, starting from the frame $I_0 + 1$. For relative scaling coefficients, we use channel-wise scaling standard deviation σ of ground truth frames, which vary between different prompts.

5 Experimental Results

We benchmark VICON against two state-of-the-art sequence-to-sequence models: DPOT [27] (122M parameters) and MPP [26] (AViT-B architecture, 116M parameters). The vanilla ICON, which would require processing over 114K tokens per frame (128×128×7), exceeds our available GPU memory and is thus computationally infeasible for direct comparison on these datasets.

For evaluation, we use both absolute and relative L^2 RMSE (Section 4.6) on rollout predictions. Since VICON offers the flexibility of predictions with different time step strides, we evaluate our

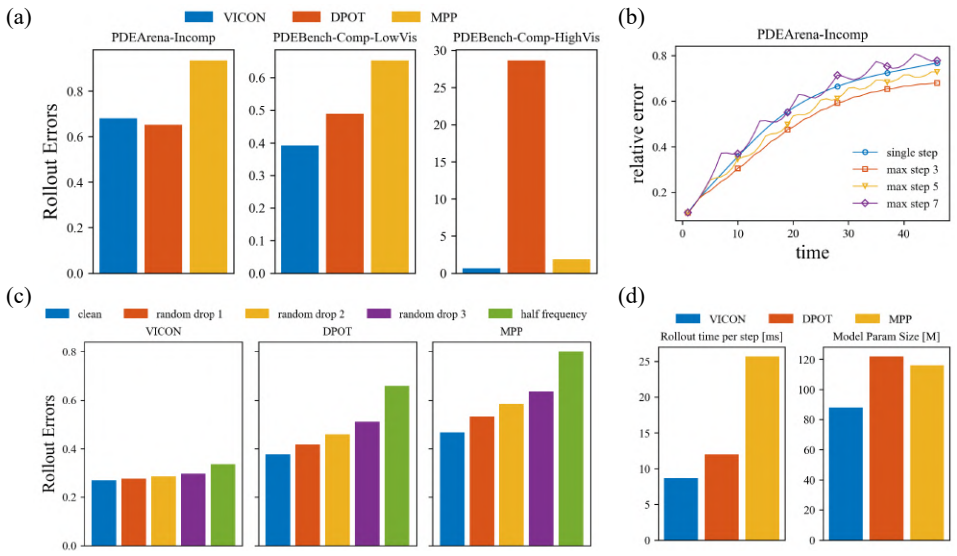

Figure 2: **Main experiment results.** (a) Last step rollout errors on 3 datasets. VICON outperforms MPP on all datasets and outperforms DPOT on 2 datasets. (b) VICON allows flexible rollout strategies to reduce error accumulation and demonstrates stride extrapolation. (c) VICON is robust to imperfect temporal measurements, while MPP and DPOT suffer from performance degradation. (d) VICON is smaller in size and has faster rollout time per step.

single trained model using both single-step and flexible-step rollout strategies (Section 4.5) during inference.

For conciseness, we present summarized plots and tables the main text, and defer complete results and visualizations to Appendix D. Ablation studies examining key design choices of VICON—including patch resolution, positional encoding, and context length—are presented in Appendix D.1.

Table 1: **Summary of Rollout Relative L^2 Error (scaled by std)** across different methods and datasets. The best results are highlighted in bold. For flexible step rollout, step 3 works best for the PDEArena-Incomp dataset.

Rollout Relative L^2 Error	Case	Ours (single step)	Ours (flexible step)	DPOT	MPP
Last step [1e-2]	PDEArena-Incomp	76.77	68.03	**65.27**	93.52
	PDEBench-Comp-LowVis	**39.11**	**39.11**	48.92	65.32
	PDEBench-Comp-HighVis	**61.41**	**61.41**	2866	185.3
All average [1e-2]	PDEArena-Incomp	56.27	48.50	**41.20**	55.95
	PDEBench-Comp-LowVis	**27.08**	**27.08**	37.72	46.68
	PDEBench-Comp-HighVis	**30.06**	**30.06**	821.9	72.37

5.1 Superior Performance on Long-term Rollout Predictions

As demonstrated in Figure 2(a), Table 1, and Figure 3, VICON consistently outperforms baseline methods on long-horizon predictions across all benchmarks—with the exception of DPOT on the PDEArena-Incomp dataset, where our performance is comparable. Overall, VICON achieves an average reduction in relative L^2 RMSE at the final timestep of 37.9% compared to DPOT and 44.7% compared to MPP.

Notably, DPOT exhibits exceptionally poor performance on the PDEBench-Comp-HighVis dataset, with an 821.9% error compared to our 30.06%. Our visualization of failure cases reveals that DPOT struggles with trajectories with small pressure values compared to the dataset average. This may stems from DPOT's lack of prompt normalization, as compressible flow's pressure channel exhibit large magnitude variations.

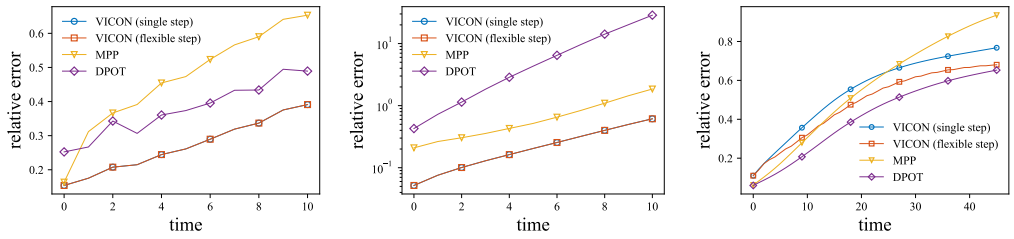

(a) PDEBench-Comp-LowVis (b) PDEBench-Comp-HighVis (c) PDEArena-Incomp

Figure 3: **Comparison of rollout errors (scaled by std) across different datasets and models.** We show errors for two VICON rollout strategies: single step rollout and flexible rollout strategy. For flexible step, step 3 works optimally for the PDEArena-Incomp dataset, while step 1 works best for PDEBench-Comp-LowVis and PDEBench-Comp-HighVis.

For the PDEArena-Incomp dataset, while VICON slightly underperforms DPOT and MPP initially, it quickly surpasses MPP and achieves comparable performance to DPOT for longer-step rollouts. This demonstrates VICON's robustness in long-term predictions. Despite DPOT's marginally better performance here, its poor performance on the PDEBench-Comp-HighVis dataset limits its applicability in multi-physics settings.

More detailed results are provided in Table 8 and Table 9 in Appendix D.

5.2 Flexible Rollout Strategies

As demonstrated in Figure 2(b) and Figure 5, VICON can select appropriate timestep strides based on each dataset's characteristics. While PDEBench-Comp-LowVis and PDEBench-Comp-HighVis perform best with single-step rollout, PDEArena-Incomp achieves optimal results with a stride of 3 using our flexible-step rollout strategy.

This dataset-dependent performance is expected: PDEBench-Comp-LowVis and PDEBench-Comp-HighVis record data with a larger timestep size and fewer total frames, making multi-stride predictions challenging. Conversely, PDEArena-Incomp records data with smaller timesteps and benefits from multi-stride prediction, as this approach reduces the rollout steps and error accumulation. As a result, VICON achieves an 11.4% error reduction in PDEArena-Incomp by selecting a balanced stride ($s_{\text{max}} = 3$).

When evaluated with unseen strides ($s_{\text{max}} = 7$), VICON maintains comparable performance to single-step strategies for PDEArena-Incomp, indicating that it extracts underlying operators through context pairs rather than memorizing dynamics. This generalization capability provides tolerance when deployed to real-world settings where device sampling rates often differ from a fixed training set—an advantage we further demonstrate in the next section.

5.3 Robustness to Imperfect Temporal Measurements

Real-world experimental measurements frequently suffer from imperfections—sampling rates may differ from training set, and frames can be missing due to device errors. Sequence-to-sequence models like MPP and DPOT require either retraining with new data or interpolation that introduces noise. In contrast, VICON elegantly handles such imperfections by forming context pairs from available frames only (Figure 1(c)). The algorithm for generating pairs with imperfect measurements appears in Appendix C.2.

We evaluate VICON against baselines on all benchmarks under two scenarios: (1) half sampling rate (dropping every other frame) and (2) random frame dropping (removing 1-3 frames per sequence). Results for the PDEBench-Comp-LowVis dataset in Figure 2(c) (with complete results in Figure 8) show that VICON experiences only 24.41% relative performance degradation compared to 71.37%-74.49% in baselines—demonstrating remarkable robustness to measurement imperfections.

5.4 Turbulence Kinetic Energy Analysis

Turbulence kinetic energy (TKE), defined as $\frac{1}{2}(\overline{\tilde{u}_x^2} + \overline{\tilde{u}_y^2})$, is a critical metric for quantifying a model's ability to capture turbulent flow characteristics. Here, $\tilde{\boldsymbol{u}} = \boldsymbol{u} - \overline{\boldsymbol{u}}$ denotes the fluctuation of velocity from its statistical equilibrium state $\overline{\boldsymbol{u}}$.

Within our datasets, only a subset of PDEBench-Comp-LowVis, specifically those initialized with fully developed turbulent fields (see Appendix D.5 of [49]), is suitable for TKE analysis. After filtering these entries, we compare the mean absolute error (MAE) of the TKE between VICON, DPOT, and MPP. Our approach achieves a TKE error of 0.016, significantly outperforming MPP's error of 0.049, while achieving performance comparable to DPOT's error of 0.012. Visualizations of TKE errors are presented in Figure 6 in Appendix D.

5.5 Benefits of Multi-Physics Joint Training

We empirically examine whether VICON benefits from a multi-physics training by comparing two strategies: (1) training a single model *jointly* on all three datasets versus (2) training *separate* models specialized for individual datasets. For fair comparison, we maintained identical batch sizes across all trainings while adjusting the steps for separate training to be slightly more than one-third of the joint training duration, ensuring **comparable total computational costs** between approaches.

As shown in Figure 7, joint training significantly outperforms separate training across all three datasets. We attribute this performance gain to the underlying physical similarities across these fluid dynamics problems, where exposure to diverse yet related flow patterns enhances the model's generalization ability.

5.6 Computational Efficiency

In Figure 2(d) and Table 11, we compare the computational resources required by VICON and baselines. Our model demonstrates superior efficiency across multiple metrics. Compared to MPP, VICON requires approximately one-third of the inference time per frame while using 75% of the total parameters. VICON also outperforms DPOT, requiring 28% fewer parameters and 28% less inference time.

6 Conclusion and Future Works

We present VICON, a vision-transformer-based in-context operator network that efficiently processes dense physical fields through patch-wise operations. VICON overcomes the computational burden of original in-context operator networks in higher spatial dimensions while preserving the flexibility to extract multiphysics dynamics from few-shot contexts.

Our comprehensive experiments demonstrate that VICON achieves superior performance in long-term predictions, reducing the averaged last-step rollout error by 37.9% compared to DPOT and 44.7% compared to MPP, while requiring only 72.5% and 34.8% of their respective inference times. The model supports flexible rollout strategies with varying timestep strides, enabling natural application to imperfect real-world measurements where sampling frequencies differ or frames are randomly dropped—scenarios where VICON experiences only 24.41% relative performance degradation compared to 71.37%-74.49% degradation in baseline models.

Despite these advances, several challenges remain for future investigation. We emperically showed in Section 5.5 the benefits of multi-physics training, yet scaling to larger and more diverse datasets presents practical challenges. Specifically, generating high-fidelity physics simulation data across multiple domains requires both substantial computational resources and specialized domain expertise. Furthermore, the current approach does not yet extend to 3D applications, as token sequence length would grow cubically, exceeding our computational budget. The channel-union approach is also limited when incorporating domains beyond fluid dynamics with fundamentally different state variables. Finally, adapting VICON to handle irregular domains such as graphs or meshes would broaden its applications to areas like solid mechanics and molecular dynamics. Addressing these challenges will advance the promising paradigm of in-context learning for a broader range of physical systems.

References

[1] J. K. Gupta and J. Brandstetter. Towards multi-spatiotemporal-scale generalized pde modeling. *arXiv preprint arXiv:2209.15616*, 2022.

[2] A. Sanchez-Gonzalez, J. Godwin, T. Pfaff, R. Ying, J. Leskovec, and P. Battaglia. Learning to simulate complex physics with graph networks. In *International conference on machine learning*, pages 8459–8468. PMLR, 2020.

[3] M. Lino, S. Fotiadis, A. A. Bharath, and C. D. Cantwell. Multi-scale rotation-equivariant graph neural networks for unsteady eulerian fluid dynamics. *Physics of Fluids*, 34(8):087110, 2022.

[4] Y. Cao, M. Chai, M. Li, and C. Jiang. Efficient learning of mesh-based physical simulation with bi-stride multi-scale graph neural network. In *International Conference on Machine Learning*, pages 3541–3558, 2023.

[5] S. Cao. Choose a transformer: Fourier or galerkin. *Advances in neural information processing systems*, 34:24924–24940, 2021.

[6] Y. Dang, Z. Hu, M. Cranmer, M. Eickenberg, and S. Ho. Tnt: Vision transformer for turbulence simulations. *arXiv preprint arXiv:2207.04616*, 2022.

[7] J. Jiang, G. Li, Y. Jiang, L. Zhang, and X. Deng. Transcfd: A transformer-based decoder for flow field prediction. *Engineering Applications of Artificial Intelligence*, 123:106340, 2023.

[8] T. Chen and H. Chen. Universal approximation to nonlinear operators by neural networks with arbitrary activation functions and its application to dynamical systems. *IEEE transactions on neural networks*, 6(4):911–917, 1995.

[9] T. Chen and H. Chen. Approximation capability to functions of several variables, nonlinear functionals, and operators by radial basis function neural networks. *IEEE Transactions on Neural Networks*, 6(4):904–910, 1995.

[10] L. Lu, P. Jin, G. Pang, Z. Zhang, and G. E. Karniadakis. Learning nonlinear operators via DeepONet based on the universal approximation theorem of operators. *Nature machine intelligence*, 3(3):218–229, 2021.

[11] Z. Li, N. B. Kovachki, K. Azizzadenesheli, B. liu, K. Bhattacharya, A. Stuart, and A. Anandkumar. Fourier neural operator for parametric partial differential equations. In *International Conference on Learning Representations*, 2021.

[12] N. Kovachki, Z. Li, B. Liu, K. Azizzadenesheli, K. Bhattacharya, A. Stuart, and A. Anandkumar. Neural operator: Learning maps between function spaces with applications to PDEs. *Journal of Machine Learning Research*, 24(89):1–97, 2023.

[13] Z. Li, K. Meidani, and A. B. Farimani. Transformer for partial differential equations' operator learning. *arXiv preprint arXiv:2205.13671*, 2022.

[14] Z. Li, D. Shu, and A. Barati Farimani. Scalable transformer for pde surrogate modeling. *Advances in Neural Information Processing Systems*, 36:28010–28039, 2023.

[15] O. Ovadia, A. Kahana, P. Stinis, E. Turkel, D. Givoli, and G. E. Karniadakis. Vito: Vision transformer-operator. *Computer Methods in Applied Mechanics and Engineering*, 428:117109, 2024.

[16] W. Chen, J. Song, P. Ren, S. Subramanian, D. Morozov, and M. W. Mahoney. Data-efficient operator learning via unsupervised pretraining and in-context learning. *arXiv preprint arXiv:2402.15734*, 2024.

[17] M. Herde, B. Raonić, T. Rohner, R. Käppeli, R. Molinaro, E. Bézenac, and S. Mishra. Poseidon: Efficient foundation models for pdes. *arXiv preprint arXiv:2405.19101*, 2024.

[18] Z. Zhang, C. Moya, L. Lu, G. Lin, and H. Schaeffer. Deeponet as a multi-operator extrapolation model: Distributed pretraining with physics-informed fine-tuning. *arXiv preprint arXiv:2411.07239*, 2024.

[19] Y. Liu, Z. Zhang, and H. Schaeffer. Prose: Predicting multiple operators and symbolic expressions using multimodal transformers. *Neural Networks*, 180:106707, 2024.

[20] Y. Liu, J. Sun, X. He, G. Pinney, Z. Zhang, and H. Schaeffer. Prose-fd: A multimodal pde foundation model for learning multiple operators for forecasting fluid dynamics. *arXiv preprint arXiv:2409.09811*, 2024.

[21] J. Sun, Y. Liu, Z. Zhang, and H. Schaeffer. Towards a foundation model for partial differential equation: Multi-operator learning and extrapolation. *arXiv preprint arXiv:2404.12355*, 2024.

[22] D. Jollie, J. Sun, Z. Zhang, and H. Schaeffer. Time-series forecasting, knowledge distillation, and refinement within a multimodal pde foundation model. *arXiv preprint arXiv:2409.11609*, 2024.

[23] Z. Ye, X. Huang, L. Chen, H. Liu, Z. Wang, and B. Dong. PDEformer: Towards a foundation model for one-dimensional partial differential equations. In *ICLR 2024 Workshop on AI4DifferentialEquations In Science*, 2024.

[24] C. Lorsung, Z. Li, and A. B. Farimani. Physics informed token transformer for solving partial differential equations. *Machine Learning: Science and Technology*, 5(1):015032, 2024.

[25] L. Yang, S. Liu, T. Meng, and S. J. Osher. In-context operator learning with data prompts for differential equation problems. *Proceedings of the National Academy of Sciences*, 120(39):e2310142120, 2023.

[26] M. McCabe, B. Régaldo-Saint Blancard, L. H. Parker, R. Ohana, M. Cranmer, A. Bietti, M. Eickenberg, S. Golkar, G. Krawezik, F. Lanusse, and others. Multiple physics pretraining for physical surrogate models. In *NeurIPS 2023 AI for Science Workshop*, 2023.

[27] Z. Hao, C. Su, S. Liu, J. Berner, C. Ying, H. Su, A. Anandkumar, J. Song, and J. Zhu. Dpot: Auto-regressive denoising operator transformer for large-scale pde pre-training. *arXiv preprint arXiv:2403.03542*, 2024.

[28] L. Lu, X. Meng, S. Cai, Z. Mao, S. Goswami, Z. Zhang, and G. E. Karniadakis. A comprehensive and fair comparison of two neural operators (with practical extensions) based on fair data. *Computer Methods in Applied Mechanics and Engineering*, 393:114778, 2022.

[29] S. Wang, H. Wang, and P. Perdikaris. Learning the solution operator of parametric partial differential equations with physics-informed DeepONets. *Science Advances*, 7(40):eabi8605, 2021.

[30] Z. Li, H. Zheng, N. Kovachki, D. Jin, H. Chen, B. Liu, K. Azizzadenesheli, and A. Anandkumar. Physics-informed neural operator for learning partial differential equations. *ACM/JMS Journal of Data Science*, 1(3):1–27, 2024.

[31] Z. Zhang, C. Moya, W. T. Leung, G. Lin, and H. Schaeffer. Bayesian deep operator learning for homogenized to fine-scale maps for multiscale pde. *Multiscale Modeling & Simulation*, 22(3):956–972, 2024.

[32] G. Wen, Z. Li, K. Azizzadenesheli, A. Anandkumar, and S. M. Benson. U-fno—an enhanced fourier neural operator-based deep-learning model for multiphase flow. *Advances in Water Resources*, 163:104180, 2022.

[33] X. Liu, M. Zhu, L. Lu, H. Sun, and J. Wang. Multi-resolution partial differential equations preserved learning framework for spatiotemporal dynamics. *Communications Physics*, 7(1):31, 2024.

[34] Z. Zhang, L. Wing Tat, and H. Schaeffer. Belnet: basis enhanced learning, a mesh-free neural operator. *Proceedings of the Royal Society A*, 479(2276):20230043, 2023.

[35] Z. Zhang, C. Moya, L. Lu, G. Lin, and H. Schaeffer. D2no: Efficient handling of heterogeneous input function spaces with distributed deep neural operators. *Computer Methods in Applied Mechanics and Engineering*, 428:117084, 2024.

[36] Z. Li, N. Kovachki, C. Choy, B. Li, J. Kossaifi, S. Otta, M. A. Nabian, M. Stadler, C. Hundt, K. Azizzadenesheli, and others. Geometry-informed neural operator for large-scale 3d pdes. *Advances in Neural Information Processing Systems*, 36, 2024.

[37] H. Wu, H. Luo, H. Wang, J. Wang, and M. Long. Transolver: A fast transformer solver for pdes on general geometries. *arXiv preprint arXiv:2402.02366*, 2024.

[38] T. Brown, B. Mann, N. Ryder, M. Subbiah, J. D. Kaplan, P. Dhariwal, A. Neelakantan, P. Shyam, G. Sastry, A. Askell, and others. Language models are few-shot learners. *Advances in neural information processing systems*, 33:1877–1901, 2020.

[39] H. Touvron, T. Lavril, G. Izacard, X. Martinet, M. Lachaux, T. Lacroix, B. Rozière, N. Goyal, E. Hambro, F. Azhar, and others. LLaMA: Open and efficient foundation language models. *arXiv preprint arXiv:2302.13971*, 2023.

[40] A. Ramesh, M. Pavlov, G. Goh, S. Gray, C. Voss, A. Radford, M. Chen, and I. Sutskever. Zero-shot text-to-image generation. In *International conference on machine learning*, pages 8821–8831. Pmlr, 2021.

[41] H. Schaeffer. Learning partial differential equations via data discovery and sparse optimization. *Proceedings of the Royal Society A: Mathematical, Physical and Engineering Sciences*, 473(2197):20160446, 2017.

[42] H. Wang, Y. Cao, Z. Huang, Y. Liu, P. Hu, X. Luo, Z. Song, W. Zhao, J. Liu, J. Sun, and others. Recent advances on machine learning for computational fluid dynamics: A survey. *arXiv preprint arXiv:2408.12171*, 2024.

[43] J. Sun, Z. Zhang, and H. Schaeffer. Lemon: Learning to learn multi-operator networks. *arXiv preprint arXiv:2408.16168*, 2024.

[44] H. Zhou, Y. Ma, H. Wu, H. Wang, and M. Long. Unisolver: PDE-conditional transformers are universal neural PDE solvers. In *ICLR 2025 Workshop on Foundation Models in the Wild*, 2025.

[45] L. Yang, S. Liu, and S. J. Osher. Fine-tune language models as multi-modal differential equation solvers. *arXiv preprint arXiv:2308.05061*, 2023.

[46] L. Yang and S. J. Osher. PDE generalization of in-context operator networks: A study on 1D scalar nonlinear conservation laws. *Journal of Computational Physics*, 519:113379, 2024.

[47] A. Dosovitskiy, L. Beyer, A. Kolesnikov, D. Weissenborn, X. Zhai, T. Unterthiner, M. Dehghani, M. Minderer, G. Heigold, S. Gelly, J. Uszkoreit, and N. Houlsby. An image is worth 16x16 words: Transformers for image recognition at scale. In *International Conference on Learning Representations*, 2021.

[48] Y. Bai, X. Geng, K. Mangalam, A. Bar, A. L. Yuille, T. Darrell, J. Malik, and A. A. Efros. Sequential modeling enables scalable learning for large vision models. In *Proceedings of the IEEE/CVF Conference on Computer Vision and Pattern Recognition*, pages 22861–22872, 2024.

[49] M. Takamoto, T. Praditia, R. Leiteritz, D. MacKinlay, F. Alesiani, D. Pflüger, and M. Niepert. Pdebench: An extensive benchmark for scientific machine learning. *Advances in Neural Information Processing Systems*, 35:1596–1611, 2022.

[50] A. Paszke, S. Gross, F. Massa, A. Lerer, J. Bradbury, G. Chanan, T. Killeen, Z. Lin, N. Gimelshein, L. Antiga, and others. Pytorch: An imperative style, high-performance deep learning library. *Advances in neural information processing systems*, 32, 2019.

[51] S. Li, Y. Zhao, R. Varma, O. Salpekar, P. Noordhuis, T. Li, A. Paszke, J. Smith, B. Vaughan, P. Damania, and others. Pytorch distributed: Experiences on accelerating data parallel training. *arXiv preprint arXiv:2006.15704*, 2020.

A Dataset Details

A.1 PDEArena-Incomp Dataset

The incompressible Navier-Stokes dataset comes from PDEArena [1]. The data are generated from the equation

$$\partial_t \boldsymbol{u} + \boldsymbol{u} \cdot \nabla \boldsymbol{u} = -\nabla p + \mu \Delta \boldsymbol{u} + \boldsymbol{f}, \tag{9}$$

$$\nabla \cdot \boldsymbol{u} = 0. \tag{10}$$

The space-time domain is $[0, 32]^2 \times [18, 105]$ where $dt = 1.5$ and the space resolution is 128×128. A scalar particle field is being transported with the fluids. The velocity fields satisfy Dirichlet boundary condition, and the scalar field satisfies Neumann boundary condition. The forcing term $\boldsymbol{f}$ is randomly sampled. The quantities of interest are the velocities and the scalar particle field.

A.2 PDEBench-Comp-HighVis and PDEBench-Comp-LowVis Datasets

The PDEBench-Comp-HighVis and PDEBench-Comp-LowVis datasets come from PDEBench Compressible Navier-Stokes dataset [49]. The data are generated from the equation

$$\partial_t \rho + \nabla \cdot (\rho \boldsymbol{u}) = 0, \tag{11}$$

$$\rho(\partial_t \boldsymbol{u} + \boldsymbol{u} \cdot \nabla \boldsymbol{u}) = -\nabla p + \eta \Delta \boldsymbol{u} + (\zeta + \eta/3)\nabla(\nabla \cdot \boldsymbol{u}), \tag{12}$$

$$\partial_t \left(\varepsilon + \frac{\rho u^2}{2} \right) = -\nabla \cdot \left(\left(\varepsilon + p + \frac{\rho u^2}{2} \right) \boldsymbol{u} - \boldsymbol{u} \cdot \sigma' \right). \tag{13}$$

The space-time domain is $\mathbb{T}^2 \times [0, 1]$ where $dt = 0.05$. The datasets contain different combinations of shear and bulk viscosities. We group the ones with larger viscosities into the PDEBench-Comp-HighVis dataset, and the ones with extremely small (1e-8) viscosities into the PDEBench-Comp-LowVis dataset. The PDEBench-Comp-HighVis dataset has space resolution 128×128. The PDEBench-Comp-LowVis dataset has raw space resolution 512×512 and is downsampled to 128×128 through average pooling for consistency. The quantities of interest are velocities, pressure, and density.

A.3 QOI Union and Channel Mask

Since each dataset contains different sets of quantities of interest, we take their union to create a unified representation. The unified physical field has 7 channels in total, with the following ordering:

1. Density (ρ)
2. Velocity at x direction (u_x)
3. Velocity at y direction (u_y)
4. Pressure (P)
5. Vorticity (ω)
6. Passively transported scalar field (S)
7. Node type indicator (0: interior node, 1: boundary node)

For each dataset, we use a channel mask to indicate its valid fields and only calculate loss on these channels. The node type channel is universally excluded from loss calculations across all datasets.

B Experiment Details

B.1 VICON Model Details

Here we provide key architectural parameters of VICON model implementation in Table 2.

Table 2: Model Configuration Details

Patch Configuration	
Input patch numbers	8×8
Output patch numbers	8×8
Patch resolution	16×16
Positional Encodings Shapes	
Patch positional encodings	$[64, 1024]$
Function positional encodings	$[20, 1024]$
Transformer Configuration	
Hidden dimension	1024
Number of attention heads	8
Feedforward dimension	2048
Number of layers	10
Dropout rate	0.0
Number of COND & QOI pairs	10
Number of QOI exempted from loss calculation	5

Table 3: Optimization Hyperparameters

Parameter	Value
Learning Rate Schedule	
Scheduler	Cosine Annealing with Linear Warmup
Peak learning rate	1×10^{-4}
Final learning rate	1×10^{-7}
Warmup steps	20,000
Total steps	200,000
Optimization Settings	
Optimizer	AdamW
Weight decay	1×10^{-4}
Gradient norm clip	1.0

B.2 Training Details

We implement our method in PyTorch [50] and utilize data parallel training [51] across two NVIDIA RTX 4090 GPUs. We employ the AdamW optimizer with a cosine learning rate schedule that includes a linear warmup phase. We apply gradient clipping with a maximum norm of 1.0 to ensure training stability. All optimization parameters are detailed in Table 3.

B.3 MPP Details

For a fair comparison, we retrained MPP [26] using our training dataset using the same model configurations and optimizer hyperparameters (batch size is set to be the maximum possible on our device). We evaluate MPP using the same testing setup and metric.

B.4 DPOT Details

For a fair comparison, we retrain DPOT [27] using our training dataset using the same model configurations and optimizer hyperparameters (batch size is set to be the maximum possible on our device). We evaluate DPOT using the same testing setup and metric.

Algorithm 1: GenerateSingleStepStrategy

Input: D: Number of demonstrations to use
R: Number of ground truth reference steps
T: Total steps in sequence
Output: S: Strategy list of example pairs and question pairs

```
S ← [ ]
Ei ← range(0, D)                    /* example input indices:  0,1,...,D-1 */
Eo ← range(1, D+1)                   /* example output indices:  1,2,...,D */
for i from R to T-1 do
    Qi ← i - 1                         /* question input is previous frame */
    Qo ← i                             /* question output is current frame */
    S.append((Ei, Eo), Qi, Qo)
end
return S
```

C Algorithms and Examples of Strategy Generation

C.1 Strategy with Full Temporal Sequence

Algorithm for single-step strategy. Algorithm 1 presents our approach for generating single-step rollout strategies when all temporal frames are available. This strategy maintains a fixed stride of 1 between consecutive frames, providing stable but potentially error-accumulating predictions.

Algorithm for flexible-step strategy. Algorithm 2 describes our approach for generating flexible-step strategies with variable strides up to a maximum value. This approach reduces the total number of rollout steps required, potentially mitigating error accumulation for long sequences.

Rollout Strategy Example. We demonstrate two rollout strategies in Tables 4 and 5, showing single-step and flexible-step strategies, respectively. In both cases, the initial frames span from time step 0 to 9, and we aim to predict the trajectory up to time step 20.

As shown in Table 5, the flexible-step strategy initially uses smaller strides to build sufficient examples, then employs maximum strides for later rollouts, as detailed in Section 4.5. We note that repeated in-context examples appear in Table 5, which is common when the maximum stride is large and the initial frames cannot form enough examples. While the number of in-context examples in VICON is flexible and our model can accommodate fewer examples than the designed length, our preliminary experiments indicate that the model performs better with more in-context examples, even when some examples are repeated.

C.2 Strategy with Imperfect Temporal Sequence

When facing imperfect temporal sampling where certain frames are missing, we can still form valid demonstration pairs from the available frames. Algorithm 3 presents this adaptive pair selection process, which serves as a fundamental building block for all strategy generation algorithms in scenarios with irregular temporal data.

Algorithm for single-step strategy with drops. Algorithm 4 extends the single-step strategy to handle scenarios where frames are missing from the input sequence, adaptively forming strategies from available frames while maintaining the fixed stride constraint.

Algorithm for flexible-step strategy. Algorithm 5 presents our solution for generating flexible-step rollout strategies when frames are missing, dynamically selecting appropriate strides based on available frames and previous predictions.

Rollout Strategy Example with Missing Frames. Tables 6 and 7 illustrate our adaptive strategies when frames 2, 5, and 9 are missing from the initial sequence (with all other settings identical to those in Appendix C.1). The tables demonstrate single-step and flexible-step (max stride: 3)

Algorithm 2: GenerateFlexibleStepStrategy

Input: D: Number of demonstrations to use
R: Number of ground truth reference steps
M: Maximum stride between pairs
T: Total steps in sequence
Output: S: Strategy list of example pairs and question pairs

```
/* Require R >= M + 1 to ensure examples exist for each stride        */
S ← [ ]
Ec ← {}                          /* example condition indices by stride */
Eq ← {}                             /* example query indices by stride */
/* Prepare example pairs for each stride                              */
for s from 1 to M do
    Nd ← min(D, R - s)                /* available examples for this stride */
    Eqo ← range(R - Nd, R)                    /* output indices for examples */
    /* If we need more examples than available, repeat them           */
    reps ← ⌈D / Nd⌉                                    /* ceiling division */
    Eqo ← repeat(Eqo, reps)[0:D]                  /* repeat and truncate to D */
    Eqo.sort()                                     /* ensure increasing order */
    Ec[s] ← Eqo - s            /* input indices are s steps before outputs */
    Eq[s] ← Eqo                                    /* store output indices */
end
/* Generate rollout strategy                                          */
for i from R to T-1 do
    dist ← i - R + 1                  /* distance from last reference frame */
    s ← min(dist, M)                           /* select appropriate stride */
    Qi ← i - s                                  /* question input index */
    Qo ← i                                     /* question output index */
    S.append((Ec[s], Eq[s]), Qi, Qo)
end
return S
```

Table 4: Single-step Rollout Strategy Example

Rollout index	Examples (COND, QOI)	Question COND	Predict QOI
1	(0,1) (1,2) (2,3) (3,4) (4,5) (5,6) (6,7) (7,8) (8,9)	9	10
2	(0,1) (1,2) (2,3) (3,4) (4,5) (5,6) (6,7) (7,8) (8,9)	10	11
3	(0,1) (1,2) (2,3) (3,4) (4,5) (5,6) (6,7) (7,8) (8,9)	11	12
4	(0,1) (1,2) (2,3) (3,4) (4,5) (5,6) (6,7) (7,8) (8,9)	12	13
5	(0,1) (1,2) (2,3) (3,4) (4,5) (5,6) (6,7) (7,8) (8,9)	13	14
6	(0,1) (1,2) (2,3) (3,4) (4,5) (5,6) (6,7) (7,8) (8,9)	14	15
7	(0,1) (1,2) (2,3) (3,4) (4,5) (5,6) (6,7) (7,8) (8,9)	15	16
8	(0,1) (1,2) (2,3) (3,4) (4,5) (5,6) (6,7) (7,8) (8,9)	16	17
9	(0,1) (1,2) (2,3) (3,4) (4,5) (5,6) (6,7) (7,8) (8,9)	17	18
10	(0,1) (1,2) (2,3) (3,4) (4,5) (5,6) (6,7) (7,8) (8,9)	18	19
11	(0,1) (1,2) (2,3) (3,4) (4,5) (5,6) (6,7) (7,8) (8,9)	19	20

approaches, respectively, highlighting how our algorithm dynamically selects appropriate example pairs to maintain prediction capability despite missing some temporal samplings.

D Additional Experimental Results.

D.1 Ablation Studies

Impact of Patch Resolutions. We conducted ablation studies on patch resolution by varying patch sizes (8, 16, 32, 64) to find a balance between spatial granularity and computational resource constraint. While smaller patches theoretically capture finer details, they generate longer token sequences, hitting memory caps due to transformer's quadratic complexity. For patches smaller

Table 5: Flexible-step Rollout Strategy Example ($s_{\max} = 5$)

Rollout index	Examples (COND, QOI)	Question COND	Predict QOI
1	(0,1) (1,2) (2,3) (3,4) (4,5) (5,6) (6,7) (7,8) (8,9)	9	10
2	(0,2) (0,2) (1,3) (2,4) (3,5) (4,6) (5,7) (6,8) (7,9)	9	11
3	(0,3) (0,3) (1,4) (1,4) (2,5) (3,6) (4,7) (5,8) (6,9)	9	12
4	(0,4) (0,4) (1,5) (1,5) (2,6) (2,6) (3,7) (4,8) (5,9)	9	13
5	(0,5) (0,5) (1,6) (1,6) (2,7) (2,7) (3,8) (3,8) (4,9)	9	14
6	(0,5) (0,5) (1,6) (1,6) (2,7) (2,7) (3,8) (3,8) (4,9)	10	15
7	(0,5) (0,5) (1,6) (1,6) (2,7) (2,7) (3,8) (3,8) (4,9)	11	16
8	(0,5) (0,5) (1,6) (1,6) (2,7) (2,7) (3,8) (3,8) (4,9)	12	17
9	(0,5) (0,5) (1,6) (1,6) (2,7) (2,7) (3,8) (3,8) (4,9)	13	18
10	(0,5) (0,5) (1,6) (1,6) (2,7) (2,7) (3,8) (3,8) (4,9)	14	19
11	(0,5) (0,5) (1,6) (1,6) (2,7) (2,7) (3,8) (3,8) (4,9)	15	20

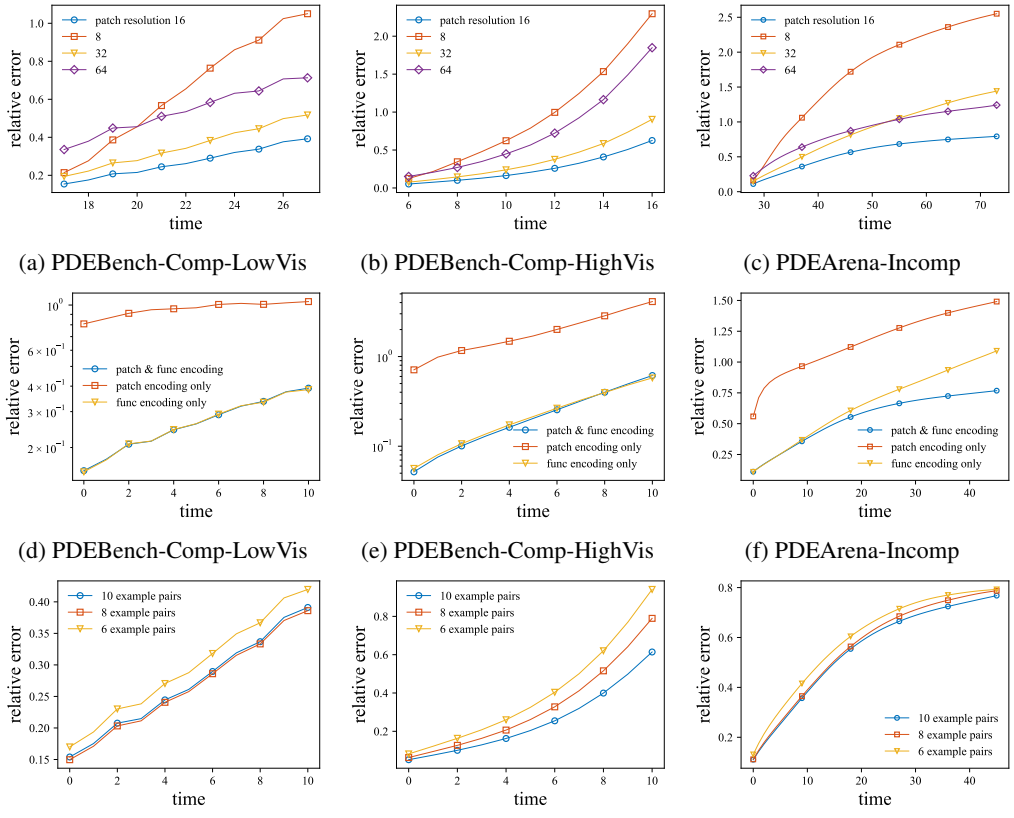

(a) PDEBench-Comp-LowVis (b) PDEBench-Comp-HighVis (c) PDEArena-Incomp

(d) PDEBench-Comp-LowVis (e) PDEBench-Comp-HighVis (f) PDEArena-Incomp

(g) PDEBench-Comp-LowVis (h) PDEBench-Comp-HighVis (i) PDEArena-Incomp

Figure 4: Ablation studies across the three datasets. **Top row (a-c):** Impact of patch resolutions $(8, 16, 32, 64)$ showing optimal performance at patch size 16. **Middle row (d-f):** Effect of different positional encoding combinations. **Bottom row (g-i):** Performance variation with different context lengths (6, 8, 10 pairs).

Algorithm 3: GetAvailablePairs

Input: D: Number of demonstrations needed
dt: Desired time stride between pairs
Fa: List of indices of available frames
Output: P: List of input-output index pairs with the specified stride

```
Fa.sort()
P ← [ ]                                          /* Initialize empty pairs list */
/* Find all pairs with stride dt                                                */
for i from 0 to len(Fa) - 1 do
    for j from i + 1 to len(Fa) - 1 do
        if Fa[j] - Fa[i] == dt then
            P.append((Fa[i], Fa[j]))
        end
    end
end
if P is empty then
    return [ ]
end
/* If we don't have enough unique pairs, repeat them                            */
if len(P) < D then
    reps ← ⌈D / len(P)⌉                                   /* ceiling division */
    RP ← repeat(P, reps)[0:D]                /* repeat pairs and truncate to D */
    P ← RP
end
return P
```

than 16×16, we had to reduce token dimensions (1024→512) and feedforward dimensions (from 2048 to 1024), while patches below 8×8 remained infeasible even with mixed precision training. Figure 4(a-c) shows that patch size 16 achieves optimal performance across all datasets—balancing sequence length and representational capacity. Performance degradation with coarser patches (32, 64) aligns with expectations, while degradation with finer patches stems from the necessary reduction in hidden dimensions, highlighting a fundamental challenge in scaling to 3D applications.

Positional Encodings. We evaluated different combinations of positional encodings as shown in Figure 4(d-f). Our architecture employs two types of encodings: patch position encodings (for spatial relationships between patches) and function encodings (differentiating input/output in different pairs) (Section 4.2).

The results demonstrate that including both encoding types consistently yields the best performance across all datasets. Notably, function encodings have a more significant impact than patch encodings, highlighting the importance of distinguishing between the condition and qoi beyond what causal masking (equation 6) provides.

The impact of patch encodings varies across datasets: they show minimal effect on the PDEBench datasets (PDEBench-Comp-LowVisand PDEBench-Comp-HighVis) yet significantly improve performance on PDEArena-Incomp. We attribute this to the different stiffness of these systems. In compressible flows (PDEBench), spatial interactions naturally decay with distance, creating consistent and monotonic spatial correlations between patches. In contrast, Navier-Stokes equations exhibit infinite stiffness where correlations between any spatial locations are instantaneous and determined by the global velocity field, creating non-monotonic and case-dependant relationships. Explicitly encoding spatial positions therefore becomes particularly beneficial for PDEArena-Incomp, as it reduces the learning complexity for these non-local dependencies.

Varying Context Length. We investigated how the number of in-context examples affects model performance, as shown in Figure 4(g-i). Following insights from the original ICON work [25], we evaluated context lengths of 6, 8, and 10 pairs, balancing performance against computational efficiency. The results show that 10 in-context examples deliver significantly better results for

Algorithm 4: GenerateSingleStepStrategyWithDrops

Input: D: Number of demonstrations to use
S: Fixed stride between pairs
T: Total steps in sequence
Fa: List of indices of available frames
Output: St: Strategy list of (E, Qi, Qo) tuples

St ← [ ]
Fa.sort()
Fs ← Fa[-1] `/* the starting frame for rollout */`
P ← GetAvailablePairs(D, S, Fa) `/* pairs with fixed stride */`
if *P is empty* **then**
  return [ ] `/* No available pairs with the specified stride */`
end
Fc ← Fa.copy() `/* accumulated frames (current + predicted) */`
for *i from (Fs + 1) to (T - 1)* **do**
  Ci ← i - S `/* potential condition index */`
  if *Ci ∉ Fc* **then**
    continue `/* Cannot predict frame i with stride S */`
  end
  Pdt ← P[s] `/* The example pairs for predicting frame i */`
  Qi ← i - s `/* question input index */`
  Qo ← i `/* question output index */`
  S.append(Pdt, Qi, Qo)
  Fc.append(Qo) `/* The predicted frame can be used for future steps */`
end
return St

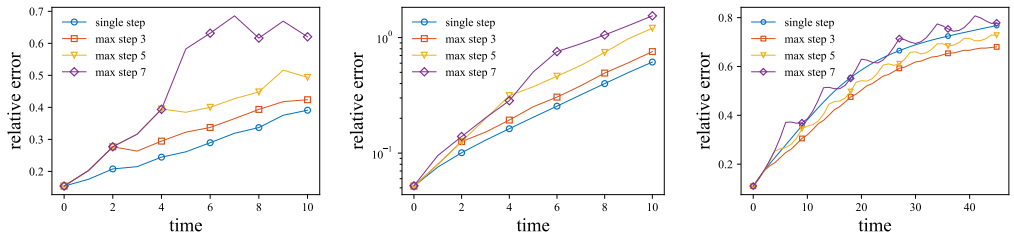

(a) PDEBench-Comp-LowVis (b) PDEBench-Comp-HighVis (c) PDEArena-Incomp

Figure 5: Comparison of rollout errors across different datasets, using single-step and flexible-step strategies with varying maximum step sizes ($s_{\max} = 1, 3, 5, 7$).

PDEBench-Comp-LowVis compared to shorter contexts, while for the remaining datasets, 10 and 8 in-context examples perform similarly (both outperforming 6 examples).

D.2 More Results and Visualizations

Detailed Results. Tables 8 and 9 summarize the relative and absolute L^2 rollout errors across different timesteps for all evaluated models on the three datasets.

Generalization to different timestep strides. Figure 5 illustrates VICON's performance with varying timestep strides ($s_{\max} = 1, 3, 5, 7$) across all three datasets, demonstrating the model's ability to adapt to different temporal resolutions without retraining.

Turbulence Kinetic Energy (TKE) Predictions. Figure 6 displays the visualization of TKE fields for ground truth and model predictions, highlighting VICON's superior ability to preserve critical turbulent flow structures compared to baseline approaches.

Algorithm 5: GenerateFlexibleStepStrategyWithDrops

Input: D: Number of demonstrations to use
M: Maximum stride between pairs for rollout
T: Total steps in the sequence
Fa: List of indices of available frames
Output: S: Strategy list of (E, Qi, Qo) tuples, where E are the list of example pair indices (Ei, Eo) and Qi, Qo are the question and output indices

```
S ← [ ]
Fa.sort()
Fs ← Fa[-1]                                  /* the starting frame for rollout */
P ← { }                                      /* dictionary of available pairs */
for dt from 1 to M do
    Pdt ← GetAvailablePairs(D, dt, Fa)       /* pairs with stride dt in Fa */
    if Pdt is not empty then
        P[dt] ← Pdt
    end
end
Ms ← max(P.keys())                           /* maximum available stride */
Fc ← Fa.copy()                  /* accumulated frames (current + predicted) */
for i from (Fs + 1) to (T - 1) do
    dt ← i - Fs
    Mt ← min(dt, M, Ms)                      /* maximum stride for current step */
    found ← False
    for s in P.keys().sorted(reverse=True) where s ≤ Mt do
        Ci ← i - s                           /* potential condition index */
        if Ci ∈ Fc then
            /* Found a starting index to obtain frame i                  */
            found ← True
            break
        end
    end
    if not found then
        /* We cannot predict frame i                                     */
        continue
    end
    /* The example pairs for predicting frame i                          */
    Pdt ← P[s]
    Qi ← i - s                               /* question input index */
    Qo ← i                                   /* question output index */
    S.append(Pdt, Qi, Qo)
    Fc.append(Qo)
        /* The Qo frame is obtained and can be used for future rollouts */
end
return S
```

Comparison between joint training vs separate training. Figure 7 and Table 10 quantify the performance differences between jointly trained and separately trained models, demonstrating the significant advantages of multi-physics training across all datasets.

Computational Efficiency. Table 11 summarizes the computational resources required by each method, showing VICON's advantages in terms of training cost, inference speed, and model parameter count compared to both DPOT and MPP baselines.

Rollout with imperfect measurements. Figure 8 show the rollout results with imperfect temporal measurements.

Table 6: Single-step Rollout Strategy Example with Missing Frames

Rollout index	Examples (COND, QOI)	Question COND	Predict QOI
1	(0,1) (0,1) (0,1) (3,4) (3,4) (6,7) (6,7) (7,8) (7,8)	8	9
2	(0,1) (0,1) (0,1) (3,4) (3,4) (6,7) (6,7) (7,8) (7,8)	9	10
3	(0,1) (0,1) (0,1) (3,4) (3,4) (6,7) (6,7) (7,8) (7,8)	10	11
4	(0,1) (0,1) (0,1) (3,4) (3,4) (6,7) (6,7) (7,8) (7,8)	11	12
5	(0,1) (0,1) (0,1) (3,4) (3,4) (6,7) (6,7) (7,8) (7,8)	12	13
6	(0,1) (0,1) (0,1) (3,4) (3,4) (6,7) (6,7) (7,8) (7,8)	13	14
7	(0,1) (0,1) (0,1) (3,4) (3,4) (6,7) (6,7) (7,8) (7,8)	14	15
8	(0,1) (0,1) (0,1) (3,4) (3,4) (6,7) (6,7) (7,8) (7,8)	15	16
9	(0,1) (0,1) (0,1) (3,4) (3,4) (6,7) (6,7) (7,8) (7,8)	16	17
10	(0,1) (0,1) (0,1) (3,4) (3,4) (6,7) (6,7) (7,8) (7,8)	17	18
11	(0,1) (0,1) (0,1) (3,4) (3,4) (6,7) (6,7) (7,8) (7,8)	18	19

Table 7: Flexible-step Rollout Strategy Example with Missing Frames (max stride: 3)

Rollout index	Examples (COND, QOI)	Question COND	Predict QOI
1	(0,1) (0,1) (0,1) (3,4) (3,4) (6,7) (6,7) (7,8) (7,8)	8	9
2	(1,3) (1,3) (1,3) (4,6) (4,6) (4,6) (6,8) (6,8) (6,8)	8	10
3	(0,3) (0,3) (0,3) (1,4) (1,4) (3,6) (3,6) (4,7) (4,7)	8	11
4	(0,3) (0,3) (0,3) (1,4) (1,4) (3,6) (3,6) (4,7) (4,7)	9	12
5	(0,3) (0,3) (0,3) (1,4) (1,4) (3,6) (3,6) (4,7) (4,7)	10	13
6	(0,3) (0,3) (0,3) (1,4) (1,4) (3,6) (3,6) (4,7) (4,7)	11	14
7	(0,3) (0,3) (0,3) (1,4) (1,4) (3,6) (3,6) (4,7) (4,7)	12	15
8	(0,3) (0,3) (0,3) (1,4) (1,4) (3,6) (3,6) (4,7) (4,7)	13	16
9	(0,3) (0,3) (0,3) (1,4) (1,4) (3,6) (3,6) (4,7) (4,7)	14	17
10	(0,3) (0,3) (0,3) (1,4) (1,4) (3,6) (3,6) (4,7) (4,7)	15	18
11	(0,3) (0,3) (0,3) (1,4) (1,4) (3,6) (3,6) (4,7) (4,7)	16	19

Table 8: **(Comparison) Summary of Rollout Relative L^2 Error (scale by std)** for different methods across various cases. The best results are highlighted in bold.

Rollout Relative L^2 Error	**Case**	**Ours (single step)**	**Ours (flexible step)**	**DPOT**	**MPP**
Step 1 [1e-2]	PDEArena-Incomp	11.01	11.01	**5.97**	6.17
	PDEBench-Comp-LowVis	**15.40**	**15.40**	25.24	16.37
	PDEBench-Comp-HighVis	**5.18**	**5.18**	42.76	20.90
Step 5 [1e-2]	PDEArena-Incomp	22.68	20.62	**11.70**	14.81
	PDEBench-Comp-LowVis	**24.45**	**24.45**	36.05	45.45
	PDEBench-Comp-HighVis	**16.25**	**16.25**	286.3	42.93
Step 10 [1e-2]	PDEArena-Incomp	35.67	30.53	**20.74**	27.89
	PDEBench-Comp-LowVis	**37.54**	**37.54**	49.47	64.11
	PDEBench-Comp-HighVis	**49.83**	**49.83**	2016	144.46
Last step [1e-2]	PDEArena-Incomp	76.77	68.03	**65.27**	93.52
	PDEBench-Comp-LowVis	**39.11**	**39.11**	48.92	65.32
	PDEBench-Comp-HighVis	**61.41**	**61.41**	2866	185.3
All average [1e-2]	PDEArena-Incomp	56.27	48.50	**41.20**	55.95
	PDEBench-Comp-LowVis	**27.08**	**27.08**	37.72	46.68
	PDEBench-Comp-HighVis	**30.06**	**30.06**	821.9	72.37

Visualizations. We compare the output of different models in Figure 9, Figure 10, and Figure 11. Figures 12 and 13 present additional visualizations of the VICON model outputs compared to ground truth and baseline predictions, highlighting the qualitative advantages of our approach.

Table 9: **(Comparison) Summary of Rollout Absolute L^2 Error** for different methods across various cases. The best results are highlighted in bold.

Rollout L^2 Error	Case	Ours (single step)	Ours (flexible step)	DPOT	MPP
Step 1 [1e-2]	PDEArena-Incomp	5.63	5.63	**3.02**	3.12
	PDEBench-Comp-LowVis	**21.74**	**21.74**	29.47	24.47
	PDEBench-Comp-HighVis	**1.43**	**1.43**	6.22	4.73
Step 5 [1e-2]	PDEArena-Incomp	10.38	9.46	**5.37**	6.79
	PDEBench-Comp-LowVis	**31.23**	**31.23**	43.57	57.50
	PDEBench-Comp-HighVis	**2.34**	**2.34**	14.48	6.52
Step 10 [1e-2]	PDEArena-Incomp	14.65	12.55	**8.55**	11.49
	PDEBench-Comp-LowVis	**45.39**	**45.39**	59.43	78.54
	PDEBench-Comp-HighVis	**3.21**	**3.21**	25.79	8.98
Last Step [1e-2]	PDEArena-Incomp	16.50	14.56	**14.03**	19.47
	PDEBench-Comp-LowVis	**48.69**	**48.69**	63.06	85.60
	PDEBench-Comp-HighVis	**3.39**	**3.39**	27.98	9.56
All average [1e-2]	PDEArena-Incomp	16.26	14.31	**11.86**	15.77
	PDEBench-Comp-LowVis	**34.44**	**34.44**	46.60	60.68
	PDEBench-Comp-HighVis	**2.48**	**2.48**	16.86	7.04

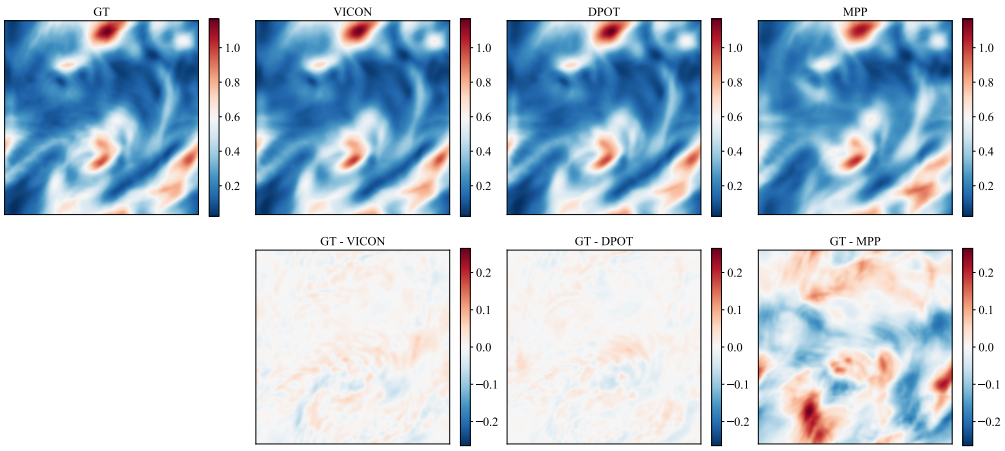

Figure 6: **Comparison of turbulence kinetic energy predictions.** (Top-left) Ground truth TKE field, (Top-right) model predictions, (Bottom) model error.

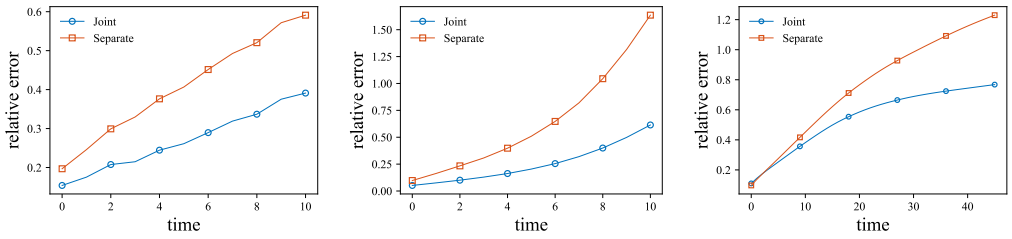

(a) PDEBench-Comp-LowVis (b) PDEBench-Comp-HighVis (c) PDEArena-Incomp

Figure 7: **Comparing rollout errors (single step, scale by std) for joint versus separate training strategies**. For separate training (individual models for each dataset), we maintain the same batch sizes as in joint training while adjusting training steps to be slightly more than one-third of the joint training duration, ensuring comparable total computational costs across both approaches.

Table 10: **Summary of Rollout Relative L^2 Error Metrics (single step, scale by std) for 2 Training Strategies**. The best results are highlighted in bold. For seperate training (a model on each dataset), each run's batch size is controlled to be the same as joint training. To ensure fair comparison, we maintain the same batch sizes as joint training for each seperate training runs while adjusting their training steps to be slightly more than one-third of the joint training duration, ensuring comparable total computational costs.

Rollout Relative L^2 Error [1e-2]	**Case**	**Joint**	**Seperate**
Step 1	PDEArena-Incomp	11.10	**9.66**
	PDEBench-Comp-LowVis	**15.61**	19.68
	PDEBench-Comp-HighVis	**5.79**	9.74
Step 5	PDEArena-Incomp	**23.00**	24.09
	PDEBench-Comp-LowVis	**24.56**	37.63
	PDEBench-Comp-HighVis	**19.73**	39.81
Step 10	PDEArena-Incomp	**36.18**	41.66
	PDEBench-Comp-LowVis	**37.47**	57.17
	PDEBench-Comp-HighVis	**57.88**	131.6
Last Step	PDEArena-Incomp	**77.81**	123.0
	PDEBench-Comp-LowVis	**39.03**	59.11
	PDEBench-Comp-HighVis	**71.17**	163.5
All average	PDEArena-Incomp	**56.26**	76.35
	PDEBench-Comp-LowVis	**27.08**	40.75
	PDEBench-Comp-HighVis	**30.06**	65.19

Table 11: **(Comparison) Summary of Resource and Timing Metrics** for different methods.

Resource and Timing Metrics	**Ours**	**DPOT**	**MPP**
Training cost [GPU hrs]	58	70	64
Rollout time per step [ms]	8.7	12.0	25.7
Model Param Size	88M	122M	116M

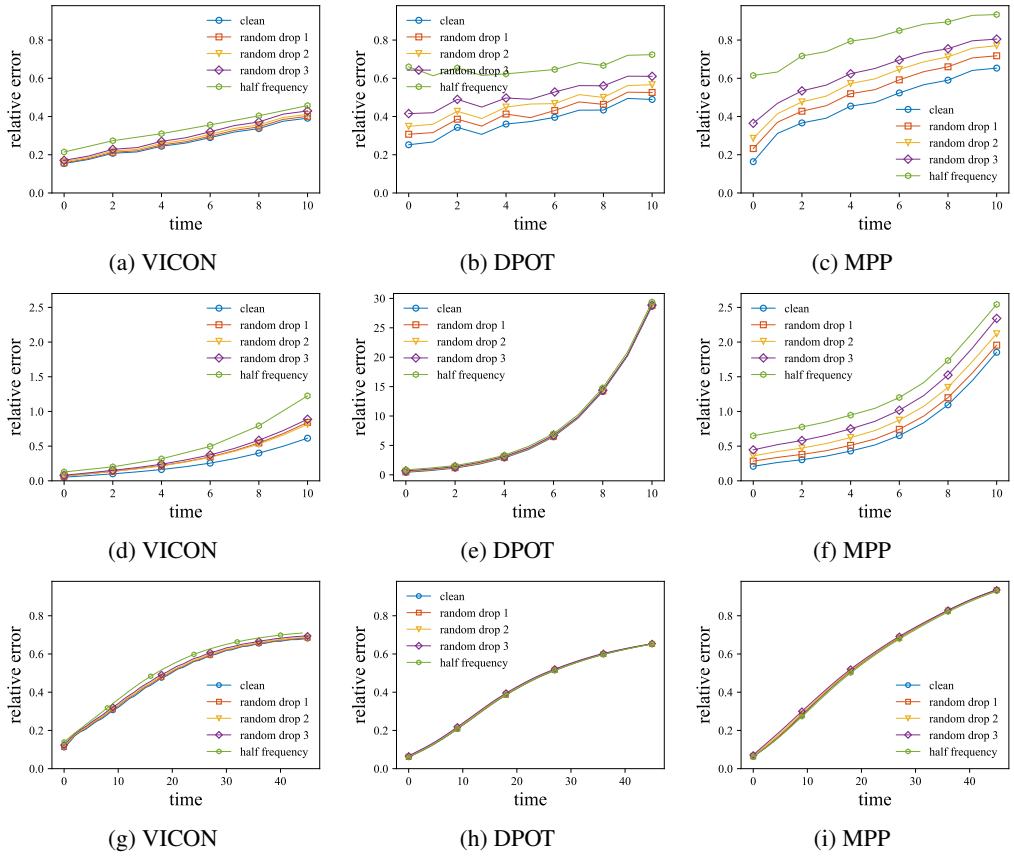

(a) VICON (b) DPOT (c) MPP

(d) VICON (e) DPOT (f) MPP

(g) VICON (h) DPOT (i) MPP

Figure 8: **Comparison of rollout errors (scale by std) with different input data noise levels across all datasets.** Each column (left to right) shows VICON, DPOT, and MPP models, while each row (top to bottom) represents PDEBench-Comp-LowVis, PDEBench-Comp-HighVis, and PDEArena-Incomp datasets. For MPP and DPOT which require fixed dt and context window, interpolation is used to generate missing frames, while VICON can directly handle irregular temporal data without interpolation.

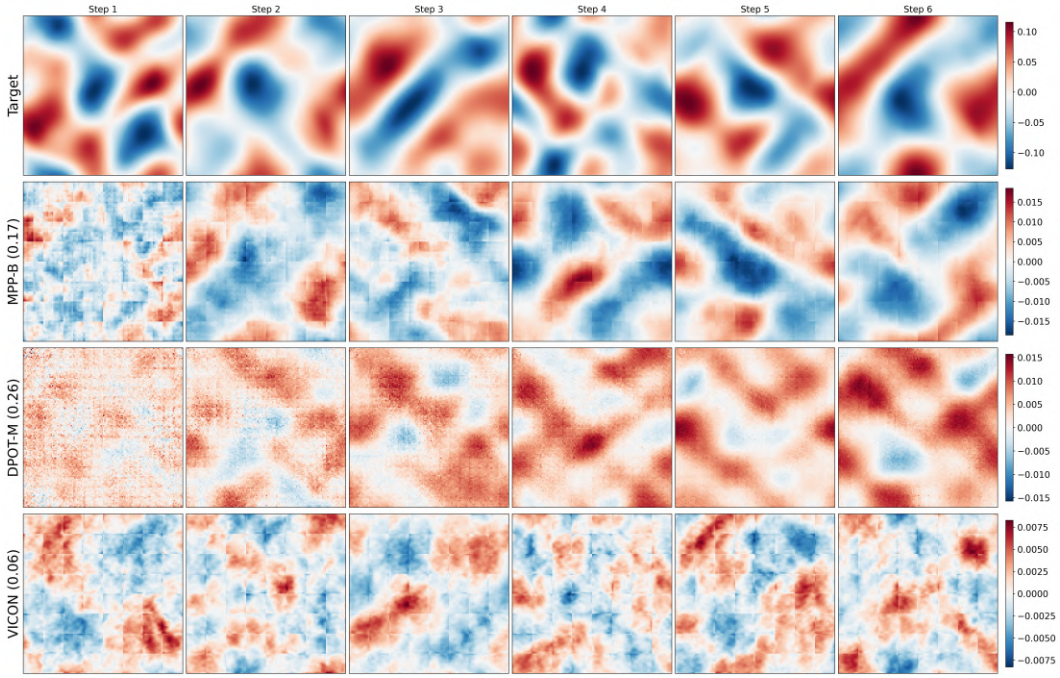

Figure 9: **Comparing outputs from different models.** The target is the first 6 output steps from PDEBench-Comp-HighVis dataset (x-velocity channel). For each model(each row), we display the difference between target and model output. Errors (rescale by std) for the full trajectory are listed after the model names.

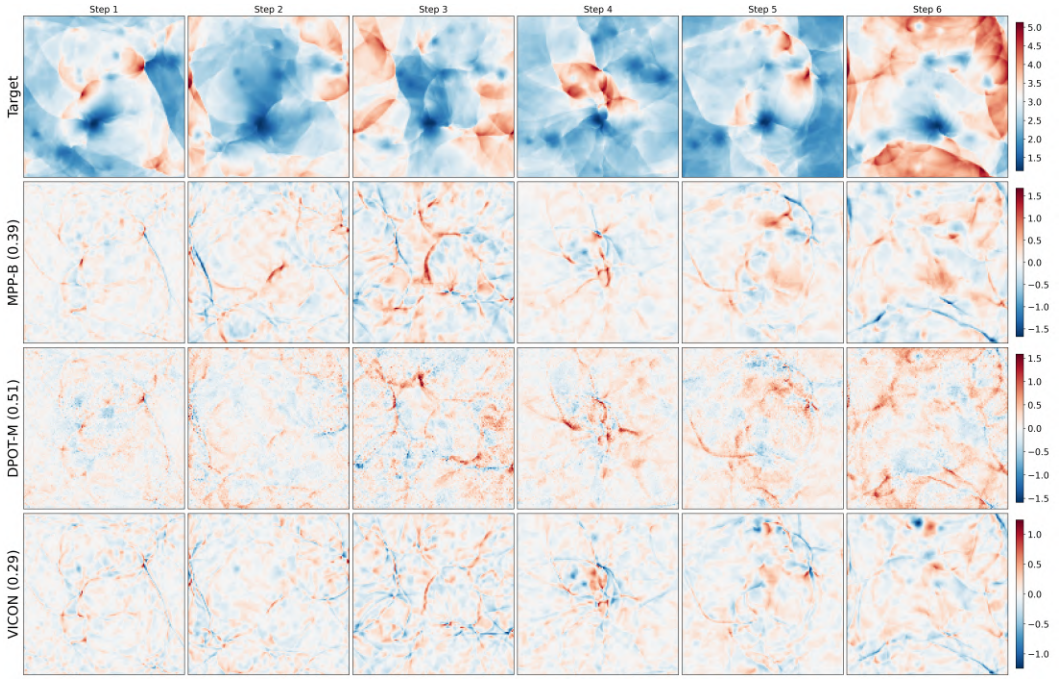

Figure 10: **Comparing outputs from different models.** The target is the first 6 output steps from PDEBench-Comp-LowVis dataset (pressure channel). For each model(each row), we display the difference between target and model output. Errors (rescale by std) for the full trajectory are listed after the model names.

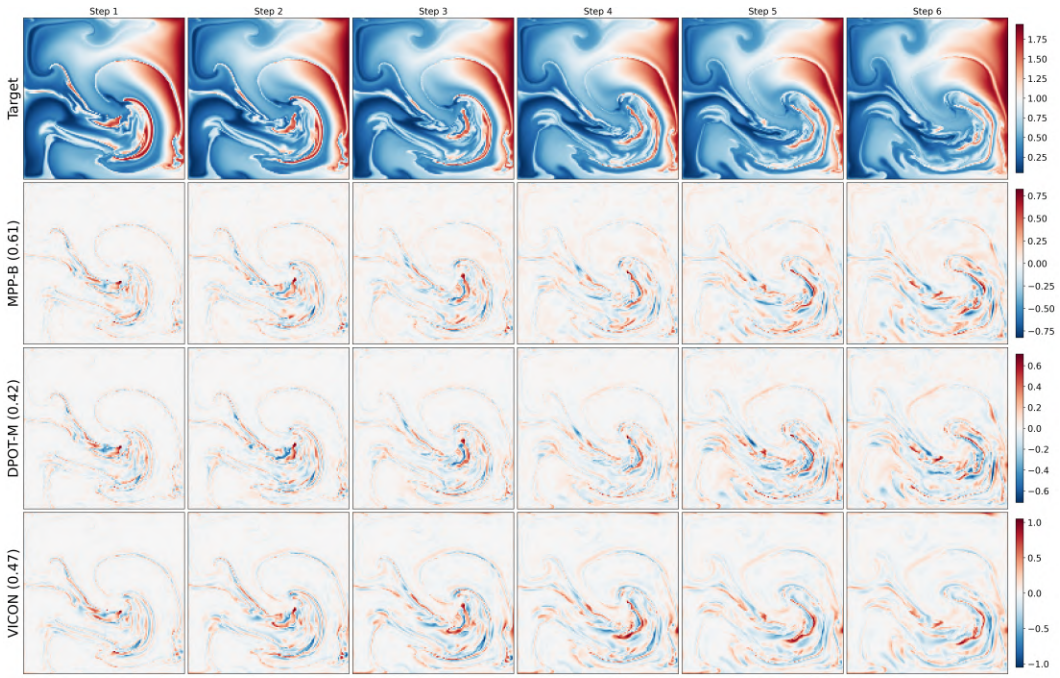

Figure 11: **Comparing outputs from different models.** The target is the first 6 output steps from PDEArena-Incomp dataset (particle density channel). For each model(each row), we display the difference between target and model output. Errors (rescale by std) for the full trajectory are listed after the model names.

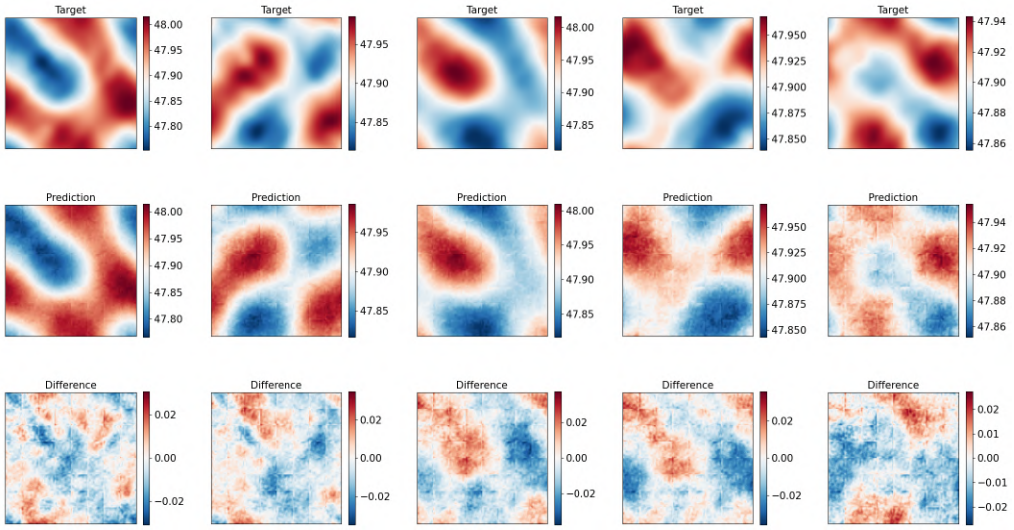

(a) A sequence of 5 output steps for PDEBench-Comp-HighVis dataset. The channel plotted is the pressure field in equation equation 12.

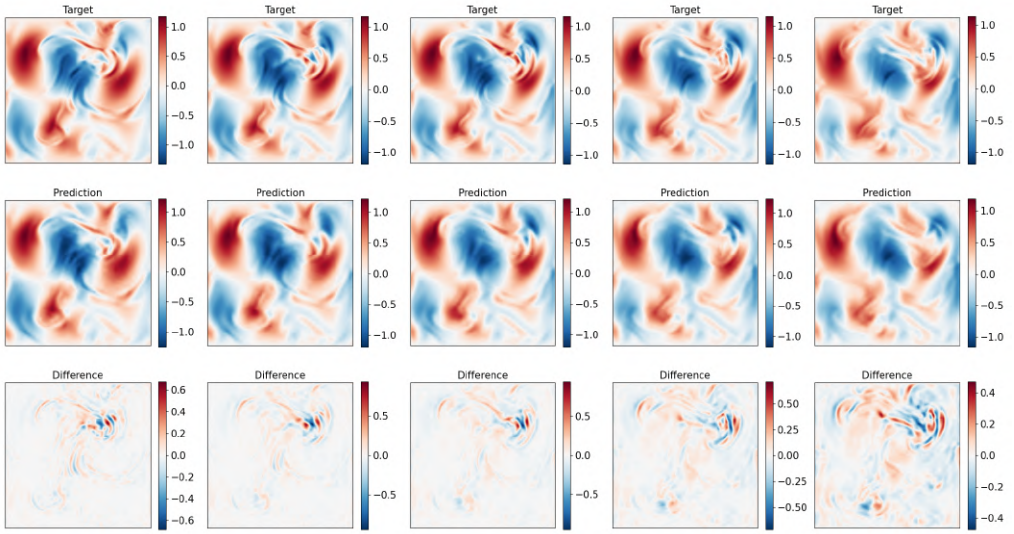

(b) A sequence of 5 output steps for PDEArena-Incomp dataset. The channel plotted is the x-velocity in equation equation 9.

Figure 12: **Example outputs for the VICON model.** (a) The pressure field of PDEBench-Comp-HighVis dataset, and (b) the x-velocity field of PDEArena-Incomp dataset. Each column represents a different timestep.

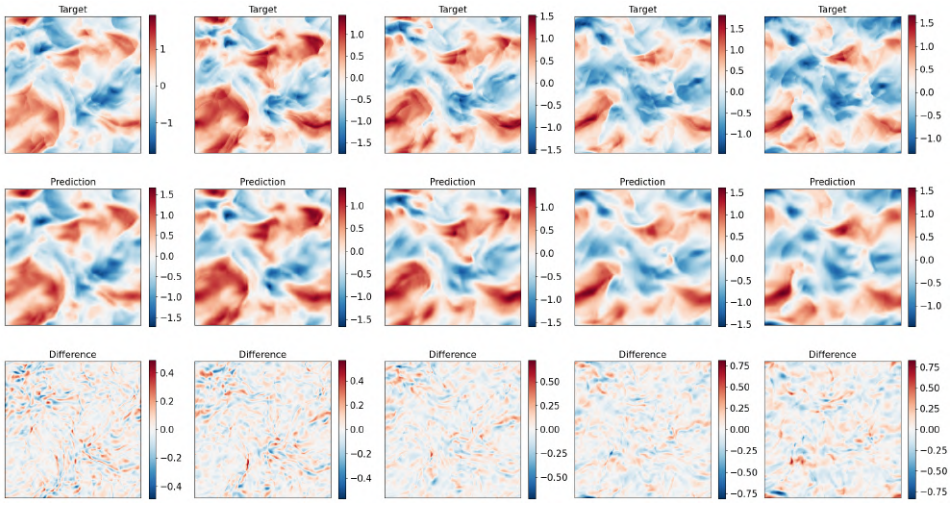

(a) The channel plotted is the y-velocity field in equation equation 9.

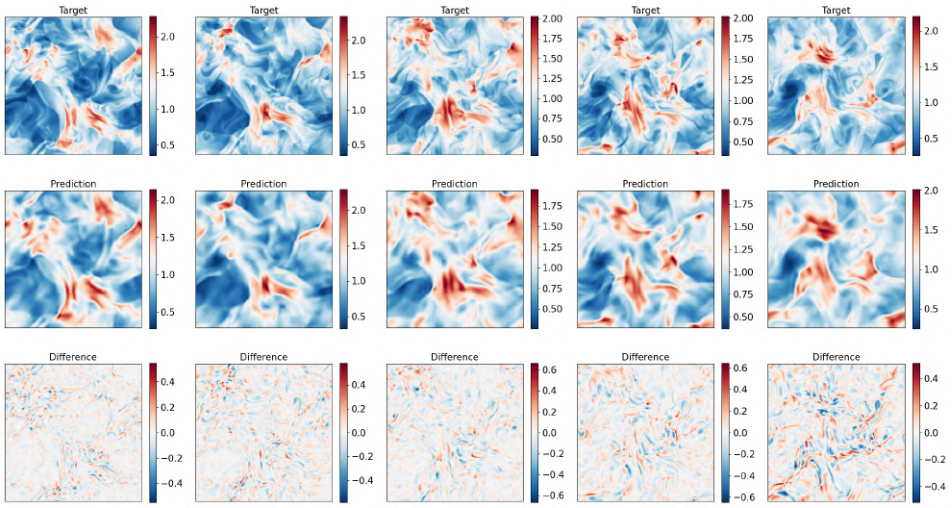

(b) The channel plotted is the density field in equation equation 9.

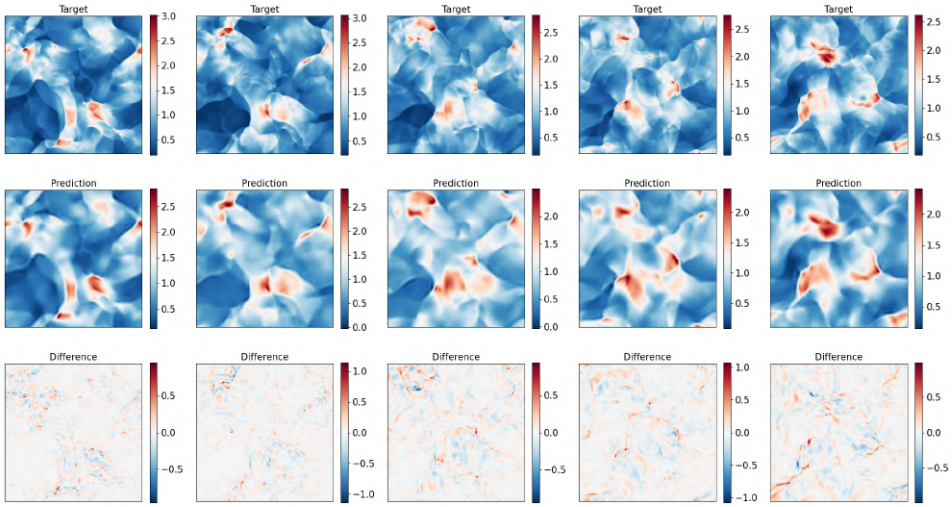

(c) The channel plotted is the pressure field in equation equation 9.

Figure 13: **More example outputs for the VICON model.** Showing 5 output steps for the PDEBench-Comp-LowVis dataset as governed by equation equation 9: (a) y-velocity, (b) density, and (c) pressure fields. Each column represents a different timestep.

NeurIPS Paper Checklist

1. **Claims**

   Question: Do the main claims made in the abstract and introduction accurately reflect the paper's contributions and scope?

   Answer: [Yes]

   Justification: The abstract and introduction Section 1 clearly state the claims made, with a contribution list at the end of the introduction.

   Guidelines:

   - The answer NA means that the abstract and introduction do not include the claims made in the paper.
   - The abstract and/or introduction should clearly state the claims made, including the contributions made in the paper and important assumptions and limitations. A No or NA answer to this question will not be perceived well by the reviewers.
   - The claims made should match theoretical and experimental results, and reflect how much the results can be expected to generalize to other settings.
   - It is fine to include aspirational goals as motivation as long as it is clear that these goals are not attained by the paper.

2. **Limitations**

   Question: Does the paper discuss the limitations of the work performed by the authors?

   Answer: [Yes]

   Justification: Our conclusion and future works Section 6 discuss the limiation, especially those related to the challanges to scale up our methodology.

   Guidelines:

   - The answer NA means that the paper has no limitation while the answer No means that the paper has limitations, but those are not discussed in the paper.
   - The authors are encouraged to create a separate "Limitations" section in their paper.
   - The paper should point out any strong assumptions and how robust the results are to violations of these assumptions (e.g., independence assumptions, noiseless settings, model well-specification, asymptotic approximations only holding locally). The authors should reflect on how these assumptions might be violated in practice and what the implications would be.
   - The authors should reflect on the scope of the claims made, e.g., if the approach was only tested on a few datasets or with a few runs. In general, empirical results often depend on implicit assumptions, which should be articulated.
   - The authors should reflect on the factors that influence the performance of the approach. For example, a facial recognition algorithm may perform poorly when image resolution is low or images are taken in low lighting. Or a speech-to-text system might not be used reliably to provide closed captions for online lectures because it fails to handle technical jargon.
   - The authors should discuss the computational efficiency of the proposed algorithms and how they scale with dataset size.
   - If applicable, the authors should discuss possible limitations of their approach to address problems of privacy and fairness.
   - While the authors might fear that complete honesty about limitations might be used by reviewers as grounds for rejection, a worse outcome might be that reviewers discover limitations that aren't acknowledged in the paper. The authors should use their best judgment and recognize that individual actions in favor of transparency play an important role in developing norms that preserve the integrity of the community. Reviewers will be specifically instructed to not penalize honesty concerning limitations.

3. **Theory assumptions and proofs**

   Question: For each theoretical result, does the paper provide the full set of assumptions and a complete (and correct) proof?

Answer: [NA]

Justification: This paper is primarily application-driven and empirical study, hence does not include theoretical results.

Guidelines:

- The answer NA means that the paper does not include theoretical results.
- All the theorems, formulas, and proofs in the paper should be numbered and cross-referenced.
- All assumptions should be clearly stated or referenced in the statement of any theorems.
- The proofs can either appear in the main paper or the supplemental material, but if they appear in the supplemental material, the authors are encouraged to provide a short proof sketch to provide intuition.
- Inversely, any informal proof provided in the core of the paper should be complemented by formal proofs provided in appendix or supplemental material.
- Theorems and Lemmas that the proof relies upon should be properly referenced.

4. **Experimental result reproducibility**

Question: Does the paper fully disclose all the information needed to reproduce the main experimental results of the paper to the extent that it affects the main claims and/or conclusions of the paper (regardless of whether the code and data are provided or not)?

Answer: [Yes]

Justification: We provide code and instructions for running the experiments in the supplementary material.

Guidelines:

- The answer NA means that the paper does not include experiments.
- If the paper includes experiments, a No answer to this question will not be perceived well by the reviewers: Making the paper reproducible is important, regardless of whether the code and data are provided or not.
- If the contribution is a dataset and/or model, the authors should describe the steps taken to make their results reproducible or verifiable.
- Depending on the contribution, reproducibility can be accomplished in various ways. For example, if the contribution is a novel architecture, describing the architecture fully might suffice, or if the contribution is a specific model and empirical evaluation, it may be necessary to either make it possible for others to replicate the model with the same dataset, or provide access to the model. In general. releasing code and data is often one good way to accomplish this, but reproducibility can also be provided via detailed instructions for how to replicate the results, access to a hosted model (e.g., in the case of a large language model), releasing of a model checkpoint, or other means that are appropriate to the research performed.
- While NeurIPS does not require releasing code, the conference does require all submissions to provide some reasonable avenue for reproducibility, which may depend on the nature of the contribution. For example
  (a) If the contribution is primarily a new algorithm, the paper should make it clear how to reproduce that algorithm.
  (b) If the contribution is primarily a new model architecture, the paper should describe the architecture clearly and fully.
  (c) If the contribution is a new model (e.g., a large language model), then there should either be a way to access this model for reproducing the results or a way to reproduce the model (e.g., with an open-source dataset or instructions for how to construct the dataset).
  (d) We recognize that reproducibility may be tricky in some cases, in which case authors are welcome to describe the particular way they provide for reproducibility. In the case of closed-source models, it may be that access to the model is limited in some way (e.g., to registered users), but it should be possible for other researchers to have some path to reproducing or verifying the results.

5. **Open access to data and code**

Question: Does the paper provide open access to the data and code, with sufficient instructions to faithfully reproduce the main experimental results, as described in supplemental material?

Answer: [Yes]

Justification: We provide code and instructions for getting the data from its original host, also the scripts to convert the downloaded data into our format. See the supplementary material.

Guidelines:

- The answer NA means that paper does not include experiments requiring code.
- Please see the NeurIPS code and data submission guidelines (`https://nips.cc/public/guides/CodeSubmissionPolicy`) for more details.
- While we encourage the release of code and data, we understand that this might not be possible, so "No" is an acceptable answer. Papers cannot be rejected simply for not including code, unless this is central to the contribution (e.g., for a new open-source benchmark).
- The instructions should contain the exact command and environment needed to run to reproduce the results. See the NeurIPS code and data submission guidelines (`https://nips.cc/public/guides/CodeSubmissionPolicy`) for more details.
- The authors should provide instructions on data access and preparation, including how to access the raw data, preprocessed data, intermediate data, and generated data, etc.
- The authors should provide scripts to reproduce all experimental results for the new proposed method and baselines. If only a subset of experiments are reproducible, they should state which ones are omitted from the script and why.
- At submission time, to preserve anonymity, the authors should release anonymized versions (if applicable).
- Providing as much information as possible in supplemental material (appended to the paper) is recommended, but including URLs to data and code is permitted.

6. **Experimental setting/details**

Question: Does the paper specify all the training and test details (e.g., data splits, hyperparameters, how they were chosen, type of optimizer, etc.) necessary to understand the results?

Answer: [Yes]

Justification: Details are included in Section 5 and Appdendix B and in the code in supplementary materials.

Guidelines:

- The answer NA means that the paper does not include experiments.
- The experimental setting should be presented in the core of the paper to a level of detail that is necessary to appreciate the results and make sense of them.
- The full details can be provided either with the code, in appendix, or as supplemental material.

7. **Experiment statistical significance**

Question: Does the paper report error bars suitably and correctly defined or other appropriate information about the statistical significance of the experiments?

Answer: [Yes]

Justification: See all tables and figures in Section 5 and Appendix B.

Guidelines:

- The answer NA means that the paper does not include experiments.
- The authors should answer "Yes" if the results are accompanied by error bars, confidence intervals, or statistical significance tests, at least for the experiments that support the main claims of the paper.

- The factors of variability that the error bars are capturing should be clearly stated (for example, train/test split, initialization, random drawing of some parameter, or overall run with given experimental conditions).
- The method for calculating the error bars should be explained (closed form formula, call to a library function, bootstrap, etc.)
- The assumptions made should be given (e.g., Normally distributed errors).
- It should be clear whether the error bar is the standard deviation or the standard error of the mean.
- It is OK to report 1-sigma error bars, but one should state it. The authors should preferably report a 2-sigma error bar than state that they have a 96% CI, if the hypothesis of Normality of errors is not verified.
- For asymmetric distributions, the authors should be careful not to show in tables or figures symmetric error bars that would yield results that are out of range (e.g. negative error rates).
- If error bars are reported in tables or plots, The authors should explain in the text how they were calculated and reference the corresponding figures or tables in the text.

8. **Experiments compute resources**

   Question: For each experiment, does the paper provide sufficient information on the computer resources (type of compute workers, memory, time of execution) needed to reproduce the experiments?

   Answer: [Yes]

   Justification: See Appendix B.2.

   Guidelines:

   - The answer NA means that the paper does not include experiments.
   - The paper should indicate the type of compute workers CPU or GPU, internal cluster, or cloud provider, including relevant memory and storage.
   - The paper should provide the amount of compute required for each of the individual experimental runs as well as estimate the total compute.
   - The paper should disclose whether the full research project required more compute than the experiments reported in the paper (e.g., preliminary or failed experiments that didn't make it into the paper).

9. **Code of ethics**

   Question: Does the research conducted in the paper conform, in every respect, with the NeurIPS Code of Ethics `https://neurips.cc/public/EthicsGuidelines`?

   Answer: [Yes]

   Justification: The authors have reviewed the NeurIPS Code of Ethics and confirmed that the research in this paper conforms with the Code.

   Guidelines:

   - The answer NA means that the authors have not reviewed the NeurIPS Code of Ethics.
   - If the authors answer No, they should explain the special circumstances that require a deviation from the Code of Ethics.
   - The authors should make sure to preserve anonymity (e.g., if there is a special consideration due to laws or regulations in their jurisdiction).

10. **Broader impacts**

    Question: Does the paper discuss both potential positive societal impacts and negative societal impacts of the work performed?

    Answer: [NA]

    Justification: This paper presents work whose goal is to advance the field of Machine Learning for Scientific Computing. There are many potential societal consequences of our work, none which we feel must be specifically highlighted here.

    Guidelines:

- The answer NA means that there is no societal impact of the work performed.
- If the authors answer NA or No, they should explain why their work has no societal impact or why the paper does not address societal impact.
- Examples of negative societal impacts include potential malicious or unintended uses (e.g., disinformation, generating fake profiles, surveillance), fairness considerations (e.g., deployment of technologies that could make decisions that unfairly impact specific groups), privacy considerations, and security considerations.
- The conference expects that many papers will be foundational research and not tied to particular applications, let alone deployments. However, if there is a direct path to any negative applications, the authors should point it out. For example, it is legitimate to point out that an improvement in the quality of generative models could be used to generate deepfakes for disinformation. On the other hand, it is not needed to point out that a generic algorithm for optimizing neural networks could enable people to train models that generate Deepfakes faster.
- The authors should consider possible harms that could arise when the technology is being used as intended and functioning correctly, harms that could arise when the technology is being used as intended but gives incorrect results, and harms following from (intentional or unintentional) misuse of the technology.
- If there are negative societal impacts, the authors could also discuss possible mitigation strategies (e.g., gated release of models, providing defenses in addition to attacks, mechanisms for monitoring misuse, mechanisms to monitor how a system learns from feedback over time, improving the efficiency and accessibility of ML).

11. **Safeguards**

    Question: Does the paper describe safeguards that have been put in place for responsible release of data or models that have a high risk for misuse (e.g., pretrained language models, image generators, or scraped datasets)?

    Answer: [NA]

    Justification: The paper is not related to LLM or generative models and hence poses no such risks.

    Guidelines:

    - The answer NA means that the paper poses no such risks.
    - Released models that have a high risk for misuse or dual-use should be released with necessary safeguards to allow for controlled use of the model, for example by requiring that users adhere to usage guidelines or restrictions to access the model or implementing safety filters.
    - Datasets that have been scraped from the Internet could pose safety risks. The authors should describe how they avoided releasing unsafe images.
    - We recognize that providing effective safeguards is challenging, and many papers do not require this, but we encourage authors to take this into account and make a best faith effort.

12. **Licenses for existing assets**

    Question: Are the creators or original owners of assets (e.g., code, data, models), used in the paper, properly credited and are the license and terms of use explicitly mentioned and properly respected?

    Answer: [Yes]

    Justification: We described the methodology to obtain dataset in Section 4.4 and Appendix A. Citations are included too. The preprocessing script for the data is in the supplementary material.

    Guidelines:

    - The answer NA means that the paper does not use existing assets.
    - The authors should cite the original paper that produced the code package or dataset.
    - The authors should state which version of the asset is used and, if possible, include a URL.

- The name of the license (e.g., CC-BY 4.0) should be included for each asset.
- For scraped data from a particular source (e.g., website), the copyright and terms of service of that source should be provided.
- If assets are released, the license, copyright information, and terms of use in the package should be provided. For popular datasets, `paperswithcode.com/datasets` has curated licenses for some datasets. Their licensing guide can help determine the license of a dataset.
- For existing datasets that are re-packaged, both the original license and the license of the derived asset (if it has changed) should be provided.
- If this information is not available online, the authors are encouraged to reach out to the asset's creators.

13. **New assets**

    Question: Are new assets introduced in the paper well documented and is the documentation provided alongside the assets?

    Answer: [NA]

    Justification: This paper does not generate new datasets. The trained model will be released upon acceptance. We will claim to use OpenCC-BY-4.0 license for the code and the model.

    Guidelines:

    - The answer NA means that the paper does not release new assets.
    - Researchers should communicate the details of the dataset/code/model as part of their submissions via structured templates. This includes details about training, license, limitations, etc.
    - The paper should discuss whether and how consent was obtained from people whose asset is used.
    - At submission time, remember to anonymize your assets (if applicable). You can either create an anonymized URL or include an anonymized zip file.

14. **Crowdsourcing and research with human subjects**

    Question: For crowdsourcing experiments and research with human subjects, does the paper include the full text of instructions given to participants and screenshots, if applicable, as well as details about compensation (if any)?

    Answer: [NA]

    Justification: All data are generated by numerical simulations (in thier original source) and no human subjects are involved in this research.

    Guidelines:

    - The answer NA means that the paper does not involve crowdsourcing nor research with human subjects.
    - Including this information in the supplemental material is fine, but if the main contribution of the paper involves human subjects, then as much detail as possible should be included in the main paper.
    - According to the NeurIPS Code of Ethics, workers involved in data collection, curation, or other labor should be paid at least the minimum wage in the country of the data collector.

15. **Institutional review board (IRB) approvals or equivalent for research with human subjects**

    Question: Does the paper describe potential risks incurred by study participants, whether such risks were disclosed to the subjects, and whether Institutional Review Board (IRB) approvals (or an equivalent approval/review based on the requirements of your country or institution) were obtained?

    Answer: [NA]

    Justification: Justification: All data are generated by numerical simulations (in thier original source) and no human subjects are involved in this research.

    Guidelines:

- The answer NA means that the paper does not involve crowdsourcing nor research with human subjects.
- Depending on the country in which research is conducted, IRB approval (or equivalent) may be required for any human subjects research. If you obtained IRB approval, you should clearly state this in the paper.
- We recognize that the procedures for this may vary significantly between institutions and locations, and we expect authors to adhere to the NeurIPS Code of Ethics and the guidelines for their institution.
- For initial submissions, do not include any information that would break anonymity (if applicable), such as the institution conducting the review.

16. **Declaration of LLM usage**

    Question: Does the paper describe the usage of LLMs if it is an important, original, or non-standard component of the core methods in this research? Note that if the LLM is used only for writing, editing, or formatting purposes and does not impact the core methodology, scientific rigorousness, or originality of the research, declaration is not required.

    Answer: [NA]

    Justification: The core method development in this research does not involve LLMs as any important, original, or non-standard components.

    Guidelines:

    - The answer NA means that the core method development in this research does not involve LLMs as any important, original, or non-standard components.
    - Please refer to our LLM policy (`https://neurips.cc/Conferences/2025/LLM`) for what should or should not be described.